Combustion and Flame 258 (2023) 113050

Contents lists available at ScienceDirect

Combustion and Flame

journal homepage: www.elsevier.com/locate/combustflame

Characterization of refill region and mixing state immediately ahead of a hydrogen-air rotating detonation using LES

Pier Carlo Nassini[a], Antonio Andreini[a,*], Myles D. Bohon[b]

[a] Department of Industrial Engineering DIEF, University of Florence, Via di Santa Marta 3, Florence 50139, Italy
[b] Chair of Pressure Gain Combustion, Technische Universität Berlin, Berlin 10623, Germany

ARTICLE INFO

Article history:
Received 17 November 2022
Revised 24 August 2023
Accepted 28 August 2023
Available online 9 September 2023

Keywords:
Rotating detonation
Hydrogen
Refill region
Non-premixed
LES

ABSTRACT

The extraordinary complexity of real Rotating Detonation Combustors (RDC) demands a deep knowledge of each phenomenon involved in the wave development and propagation. Since the reactants are typically injected separately, a key element for the combustor design optimization is understanding the refilling process and the reactants mixing. However, due to the harsh environment and high working frequencies of RDCs, the experimental diagnostics is usually limited, so high-fidelity simulations represent an essential tool to complement the measurements with detailed insights into the flow. In the present work, the non-premixed RDC installed at TU Berlin is simulated with the AVBP code by solving the fully-compressible, spatially-filtered reactive Navier-Stokes equations. The complete hydrogen and air injection system is included in the numerical model to accurately describe both the reactants mixing and the complex turbulent flow field in the resulting refill region. This study shows how both the injection system configuration and its transient interaction with the wave are fundamental for the reactants mixing, as they directly influence the refilled gas properties. Limiting the imbalances between the blockage dynamics of the fuel and oxidizer ducts and optimizing the fuel injectors can improve considerably the homogeneity of the fresh mixture, and consequently the leading shock strength and reasonably the pressure gain. In fact, the detailed analysis of the detonation front speed shown a higher instability near the chamber base for the periodic presence of unmixed reactants. Nevertheless, the unstable root of the front does not affect the whole wave speed, and remaining part propagates steadily thanks to the tangential mixture uniformity. Moreover, the local speed distribution does not appear directly related to the small-scale mixture properties, indicating a higher sensibility to the annulus curvature rather than to the local gas state.

1. Introduction

In the coming decades, continuous increases in energy demand and the share of renewable sources will require the development of flexible, highly efficient solutions to supply energy. The storage of surplus energy and the use of alternative fuels such as hydrogen are certainly two key technologies that will shape the future energy scenario. In this framework, gas turbines will hold a position in the decarbonisation thanks to their unique flexibility in operability, size and fuels [1]. A non-incremental increase of the efficiency of these machines could be potentially achieved by adopting other combustion modes involving a pressure gain during the heat addition unlocking a new generation of highly efficient gas turbines. Among all the pressure-gain devices, the Rotating Detonation Combustors (RDC) are particularly suitable for the adoption in gas turbines, as the high-frequency rotating detonation mitigates the reduction of turbine efficiency for the flow unsteadiness [2].

Although RDC technology is actively investigated by many research groups worldwide [3–9], several technical issues still need to be addressed, as their great complexity limits the experimental diagnostics which can be adopted. Different researchers have shown that an increase in performance or efficiency can be achieved with RDC, however, a positive pressure gain has still to be demonstrated [10]. Despite the lack of a well-defined method to evaluate the pressure gain, usually a high pressure loss is due to the injector, which has to quickly refill the combustor and reduce the pressure feedback from the combustion chamber into the upstream ducts. Moreover, the injector is responsible for the qual-

* Corresponding author.
E-mail address: antonio.andreini@unifi.it (A. Andreini).

https://doi.org/10.1016/j.combustflame.2023.113050

Nomenclature

Acronyms

AFR	Air to Fuel Ratio
CJ	Chapman-Jouguet
EAP	Equivalent Available Pressure
LES	Large Eddy Simulation
NSE	Navier Stokes Equations
PDF	Probability Density Function
PG	Pressure gain
PLEA	Phase-locked Ensemble Average
RDC	Rotating Detonation Combustor
ZND	Zeldovich-von Neumann-Döring

Greek symbols

δ_{half}	Half reaction thickness $[m]$
ω	Angular speed $[rad/s]$
ϕ	Generic scalar quantity $[-]$
Θ	Relative fuel injector phase $[-]$
θ	Detonation front angular distribution $[rad]$
φ	Generic scalar quantity $[-]$
ϑ	Angular coordinate $[rad]$

Latin symbols

a	Sound speed $[m/s]$
D	Detonation front normal speed $[m/s]$
d	Linear displacement of the front $[m]$
M	Mach number $[-]$
r	Radial coordinate $[m]$
S_d	Laminar flame displacement speed $[m/s]$
t	Temporal instant $[s]$
U	Unmixedness $[-]$
V	Detonation front rotation speed $[m/s]$
y	Axial coordinate $[m]$
Y_k	Mass fraction of species k $[-]$

ity of the detonable mixture as well as the flow field in the refill region, thus influencing the strength of the detonation wave and its subsequent pressure [11]. The importance of the injection system design in a RDC is clear for its performance optimisation, as it must conciliate conflicting targets and has a direct impact on the pressure gain and on the reactants mixing. Understanding the mixture characteristics in relation to the unsteady injector operation is thus fundamental for the optimization of the whole combustor.

In the past years, several numerical studies were carried out assuming perfectly premixed reactants, since this hypothesis allows for a series of problem reductions such as the use of a 2D unrolled domain, the use of Euler equations and the simplified injector models [12,13]. Although these studies were essential for describing the flow field structure associated to the rotating detonation [14] and exploring the impact of different geometrical configurations [15,16], they neglect the flow complexity due to a real injection. Indeed, practical RDCs typically adopt a non-premixed injection of the reactants directly in the combustion chamber, involving a whole series of phenomena such as the turbulent mixing of species, the dynamic coupling between the injector and the wave, and the detonation propagation in a highly turbulent, partially heterogeneous flow [10]. Thanks to the increasing computational power available, more and more studies have been carried out that include the separate reactants injection, necessarily in three dimensions [11,17–24]. Complex, non-ideal features mostly absent in the simplified models were observed in each of these investigations, such as the high vitiation of the fresh gas, parasitic combustion, and mixture stratifications [24], even leading to asymmetries in the wave strength [11] and failures [23].

These characteristics can be partially attributed to the strong velocity and composition gradients induced by the turbulent mixing in the refill region. Therefore, the turbulence model accuracy can also be expected to indirectly impact the detonation. In this regard, high-fidelity approaches such as LES, rather than URANS or hybrid simulations, should be the reference tool for the characterization of these devices, given their superior description of turbulent mixing. Nevertheless, only a few RDC studies have actually adopted LES for characterizing the turbulence fluctuations [11,18,19,23], so that the reactants mixing is usually heavily approximated. Although studies of the sub-grid effects and modelling for detonations have been delayed with respect to the efforts given to turbulent deflagration models [25], the characterization of the turbulent aerodynamics alone is crucial to provide the correct mixture properties which drive the wave development.

The main purpose of the present study is the characterization of the refilled gas properties in the TU Berlin RDC as a consequence of the radial-inward air injection and the impact on the detonation front propagation. This combustor has been extensively studied experimentally, exploring a number of phenomena that has been reasoned to be at least partially attributable to the mixing effects. Such effects include the presence of counter-rotating [26] and longitudinal [27] waves and the suppression of the wave propagation velocity relative to the Chapman-Jouget velocity [28]. Initial numerical [29] and experimental [30] studies examined steady reactant injection flow field under non-reacting conditions. However, as the rig has not been previously numerically studied in reactive conditions, the objective of this work is to study the detailed features of the unsteady reactant refill and mixing processes in a typical, canonical single wave case as representative of many of the experimental tests. From this, insight into the structure of the mixing field and the transient response of the injectors under steady operation will provide valuable insight into these coupled processes.

With this aim, an LES model is developed with specific attention to the description of the complete injection system and the turbulent reactants mixing in the refill region. A dedicated algorithm is adopted for tracking the three-dimensional evolution of the detonation front and sampling the gas properties directly ahead of the wave, allowing for a stochastic characterization of the local front speed, the refill region, and their mutual correlation. This study remarks on the importance of the transient injectors operation in the formation of the fresh mixture, suggesting design improvements to either reduce or tailor the axial and radial stratification of the mixture.

2. Test rig description

The present study is focused on the non-premixed RDC installed at TU Berlin [9]. The configuration analysed here presents an annular combustion chamber of $L = 110$ mm with straight walls and an internal radius of $r_i = 37.4$ mm and an external radius of $r_o = D/2 = 45$ mm, directly discharging into the atmosphere without any outlet restriction. The combustor is fed with the separate injection of hydrogen and air through $N = 100$ axial fuel injectors positioned at the base of the chamber and an air gap along the outer wall with height $g = 1.21$ mm, respectively, realizing a radially-inward cross-flow for the hydrogen jets (Fig. 2). The fuel injector is constituted by uniformly-spaced ($\Delta\vartheta_{inj} = 3.6^\circ$) straight channels with a diameter of $D_f = 0.5$ mm, positioned tangentially to the outer radius of the chamber. Both the air gap and the injectors are directly connected to their respective plena, where the pressure is monitored using dedicated piezo-resistive sensors.

A stoichiometric, single-wave test point of this configuration is investigated numerically and is detailed in Table 1.

In these conditions, the experimental measurements registered a 58% decrease of the total pressure at the outlet with respect to

Table 1
Main operating conditions of the analysed test point.

		Reactive case
Air manifold pressure	$bar(a)$	7.42
Fuel manifold pressure	$bar(a)$	13.12
Air temperature	K	291
Fuel temperature	K	289
Air $\dot{m}$	g/s	445
Fuel $\dot{m}$	g/s	13.3
Chamber mass flux	kg/m^2s	290
Equivalence ratio	–	1.0

the air plenum pressure [31]. In fact, the relatively small gap area and the absence of outlet restrictions are known to be detrimental for the pressure gain of this combustor, such that the test point in Table 1 has one of the highest pressure loss measured. This is to be expected given the simple, highly restrictive injector configuration used in many laboratory environments and typical for much of the published RDC literature. Therefore, the test point was chosen as the simplest, baseline condition to provide a broadly comparable and representative test case.

3. Numerical model

The flow within the RDC is governed by the fully compressible, multi-species, reactive Navier-Stokes (NS) equations. Due to the non-premixed nature of the reactants, the description of the turbulent mixing is vital for a good representation of the mixture which detonates. Therefore, in this study the NS equations are spatially-filtered in the LES formulation to accurately model the turbulence without compromising the computational demand. The sub-grid turbulent stresses deriving from the filtering operation are closed with the WALE model [32], specifically developed for wall bounded flows.

The fluid is modeled as a reactive mixture of ideal gases composed of four species, i.e. H_2, O_2, H_2O, N_2. The hydrogen-air detonation is described through a reversible global scheme, namely 4S1R :

$$H_2 + \frac{1}{2}O_2 \leftrightarrow H_2O \tag{1}$$

The net rate of progress $\mathcal{Q}$ of the reaction is calculated with an Arrhenius formulation:

$$\mathcal{Q} = A \ \exp\left(-\frac{E_a}{RT}\right)[H_2]^{n_{H_2}}[O_2]^{n_{O_2}} - k_r[H_2O] \tag{2}$$

where the reverse rate of progress k_r is calculated from the equilibrium constant. The model parameters are optimized for the present conditions, i.e. a detonation in a H_2-air mixture around the ambient pressure and temperature. The reaction order and the activation energy are estimated through the explosion theory by evaluating the ignition delay time in constant pressure 0D reactors [33] with a detailed mechanism. To match the Chapman-Jouguet speed over the whole detonability range, the formation enthalpy of H_2O is slightly increased, compensating for the altered dissociation and heat released during the combustion with respect to a complete scheme (Fig. 1(a)). Finally, the Arrhenius constant A is calibrated to match the half-reaction thickness predicted by a reference mechanism [34] around the stoichiometric composition Fig. 1(c). The chemical details of the model are summarised in Table 2 and the resulting 1D detonation profiles are shown in Fig. 1(b) against the reference scheme.

The laminar viscosity of the mixture is specified as a function of the temperature through a power law and distinct Schmidt numbers are set for the species to model the laminar diffusion, while the turbulent Schmidt and Prandtl numbers are set to 0.6. The laminar flame speed is underestimated by the present model, inducing a secondary contribution of the deflagration regime when used for modeling the oxidation. Therefore, also considering the unexplored potential interference with the detonation, no turbulent combustion model is used. These deficiencies of the chemical description are not expected to compromise the RDC analysis since the consumption rate of the reactants through the deflagration is usually at least one order of magnitude lower than through the detonation [19].

Table 2
Main parameters of the 4S1R global mechanism for a detonation in a H_2-air mixture ($p_0 = 1\ atm,\ T_0 = 298\ K$).

Model parameters		
n_{H_2}, n_{O_2}	1	
E_a/RT_0	38.8	$[-]$
A	3.1×10^{13}	$[cm^3/(mol \cdot s)]$
$\Delta H_f^{298K}(H_2O)$	−230.66	$[kJ/mol]$
Detonation properties		
$D_{CJ}(\phi = 1)$	1975	$[m/s]$
$\delta_{half}(\phi = 1)$	197	$[\mu m]$

The physical model described above is solved numerically with the cell-vertex finite-volume AVBP 7.5 code [37] developed by CERFACS and IFPEN. The Lax-Wendroff scheme [38], second-order in time and space, is used as a trade-off between accuracy and computational cost, while a localized artificial diffusivity [39] model is adopted to stabilize the code near the flow discontinuities and reduce numerical oscillations. An explicit temporal integration is carried out enforcing dynamically a maximum CFL number of 0.7, resulting in a timestep of $\Delta t \approx 6 \times 10^{-9}\ s$. The simulations were carried out on 240 cores of a HPC cluster based on Intel®Xeon ®Gold 6248 CPUs. On this hardware, the return time for the overall simulation of 4.1 ms of physical time is 650 h, i.e. 163 simulation hours per physical millisecond. The total CPU time was then about 151k CPUh.

3.1. Domain and spatial discretization

Since the detonation wave propagation and the injectors are intrinsically coupled, with the former determining the area blockage and plenum pressure feedback and the latter producing the flammable mixture, the complete geometry of the RDC including the reactant plena and ducts is considered in the simulation. The whole fluid domain is discretized with a tetrahedral mesh of 178 million elements, adopting specific refinements of 80–100 μm within the injectors and 170 μm at the chamber base to accurately reproduce the reactants turbulent mixing. The appropriate LES resolution of the turbulence in this region was verified through the Celik's quality index [40], obtaining average values around 0.8–0.9.

Indeed, a standard limitation of full RDC simulations is the general under-resolution of the reaction zone within the detonation, imposed by the computational costs and exacerbated in the case of detailed schemes involving short-living radicals. As a matter of fact, several recent studies of non-premixed RDCs [11,19,20,22–24] with detailed chemistry adopted mesh sizings around 100–200 μm, aligned to the present study. This element size is comparable to the half-reaction thickness obtained from the ZND model of 1D detonations, and in principle should not allow for correctly solving the detonation front. However, experimental [41] and numerical studies [42,43] observed a considerable broadening of the reaction region for a detonation in non-premixed reactants due to non-ideal effects and composition variations, indicating that the use of ZND detonation profiles as reference could be too conservative for practical cases.

Although the detonation front broadening is expected also in the present case, a preliminary study in a 2D detonation tube

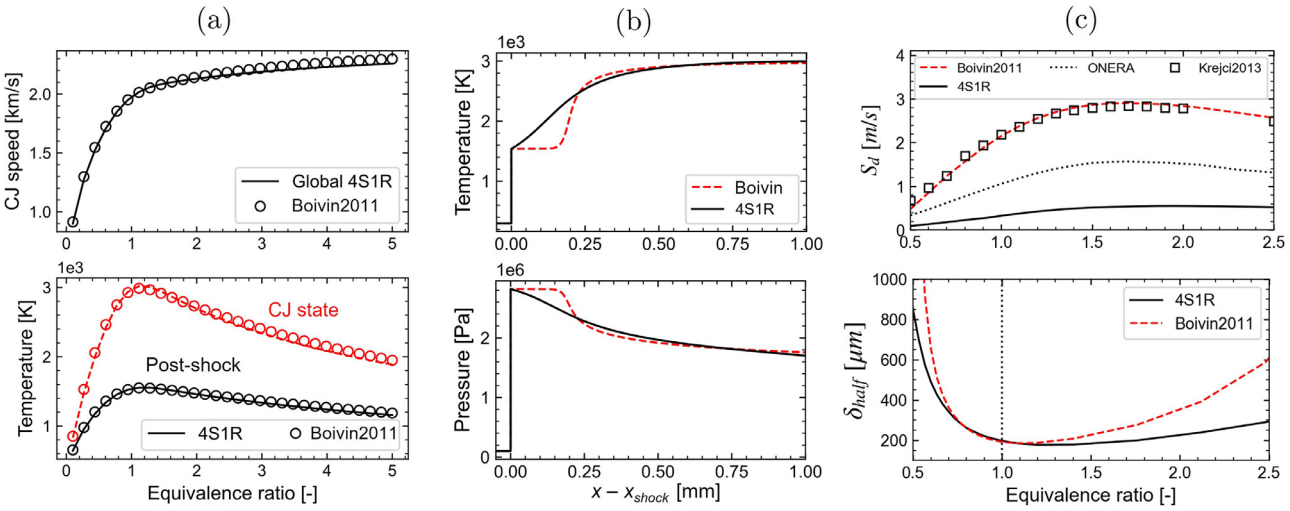

Fig. 1. Performances of the global 4S1R scheme in an atmospheric H_2-air mixture: (a) Chapman-Jouguet speed and thermodynamic states predicted by the global 4S1R scheme and a detailed scheme [34] varying the equivalence ratio; (b) static temperature and pressure profiles in a 1D CJ detonation in a stoichiometric H_2-air mixture; (c) laminar flame speed and half reaction thickness in a 1D CJ detonation. The laminar flame speed is also compared against the experimental measurements of Krejci et al. [35] and a reduced scheme by ONERA [36].

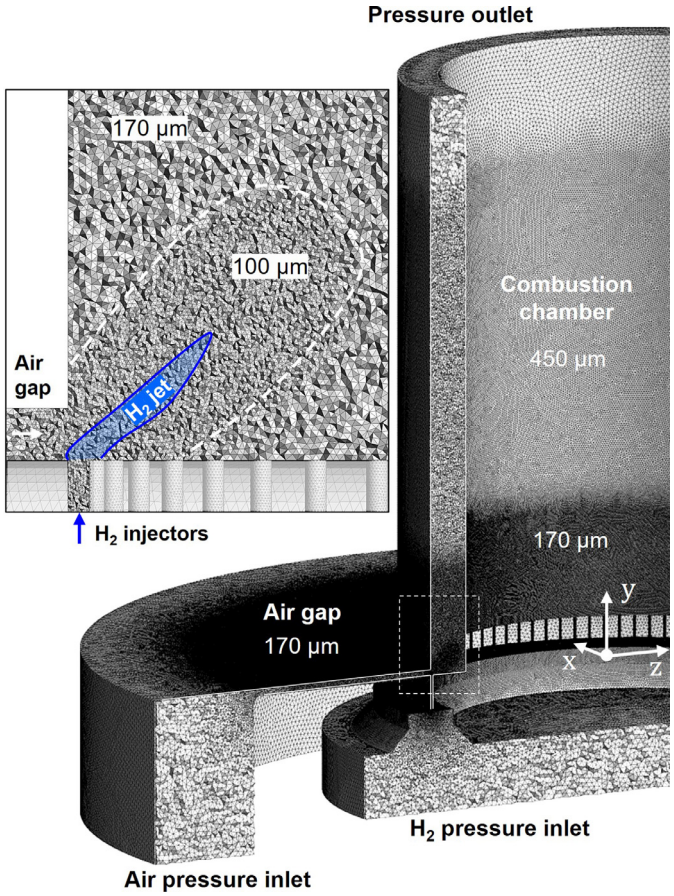

Fig. 2. Section of the mesh grid used for the simulations with the local element size and the detail of the injection.

was carried out to assess the numerical model accuracy when the detonation front is under-resolved. Both the 4S1R global scheme and a skeletal H_2-air mechanism with 9 species and 12 reactions [34] were tested to highlight the impact of the chemical model. The analysis showed that the more detailed scheme did not perform well on coarse elements ($\Delta_e \approx 0.5\delta_{half}$), and did not capture the cellular structure observed experimentally. On the other hand, the global scheme did not degenerate on coarse meshes, outperforming the skeletal scheme in the description of realistic detonation cells. This was attributed to the better discretization of species profiles and less pronounced gradients in the detonation front (Fig. 1), which reduces the mesh size requirements of the global scheme. Considering that both the schemes predicted detonation speeds comparable to the CJ value, the adoption of the 4S1R scheme on the present mesh size was considered sufficiently accurate for representing the detonation front and the resulting flow field in the combustor.

3.2. Boundary conditions and initialization

The air and hydrogen inlet boundaries are set at the base of their respective feeding plena, where the pressure is imposed through the partially non-reflecting Navier-Stokes characteristic boundary (NSCBC) conditions. At the chamber outlet, no domain extension is adopted, setting the atmospheric pressure at the exit surface using NSCBC, as the boundary condition is able to dynamically switch from a characteristic subsonic to a supersonic outlet when the local Mach number exceeds unity. The no-slip condition at the walls is modeled using turbulent adiabatic wall functions [44].

After the preliminary simulation of the non-reactive flow, a dedicated initial solution is imposed in the chamber for both initiating the detonation wave and achieving a fast stabilization of the flow within the combustor. The guessed solution is based on a 1D overdriven detonation profile and approximates a basic RDC flow field, as shown in Fig. 3.

The initiation strategy adopted has been extensively tested in preliminary 2D RDC simulations and compared against other approaches, showing that in this operating point the wave mode does not depend on the initialization, as observed during the experiments [45].

Once the detonation is initiated, about 6 wave rotations (0.75 ms) are required to completely stabilize the mass flow rate, temperature and heat release in the combustion chamber. Then, the solution fields during the following 2 ms are considered for the analysis, corresponding to about 15 revolutions of the wave.

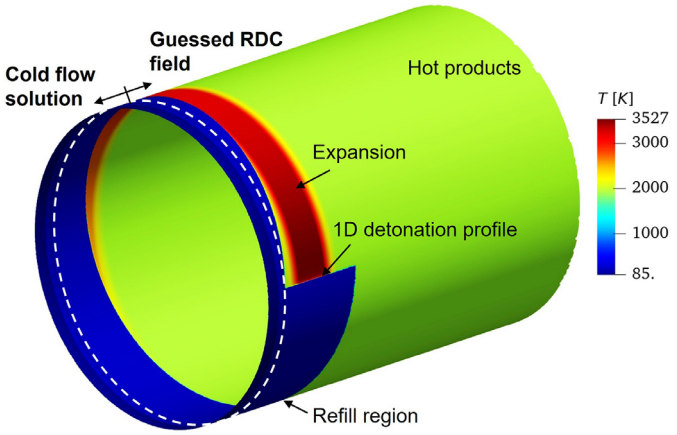

Fig. 3. Temperature distribution of the initial solution at the mid-span of the combustion chamber.

3.3. Data extraction procedure

Since the scope of the work is studying the detonation front propagation in relation to the local gas mixture, specific attention is devoted to tracking the detonation front and sampling the gas properties preceding the wave during its rotation in the combustion chamber. During the simulation, a dedicated algorithm is executed with a constant interval of $\Delta t = 3.25 \times 10^{-8}$ s (31 MHz), corresponding to roughly 4100 samples per rotation (41 per fuel channels pitch). The procedure is constituted by two steps, which can be summarised as follows:

1. **Detonation front identification:** a constant static pressure ($p =$ 9 bar) isosurface is exported and processed to discriminate the nodes laying on the frontal surface from all the others, i.e. to obtain a surface $\theta(r, y, t)$. This operation is carried out by selecting the points on the isosurface with the maximum angular position within a radial-axial half-overlapping moving window of 0.5×0.5 mm. Also, the mean angular position of the front $\theta_m(t) = \sum_{r,y}^{M} \theta(r, y, t)/M$ is calculated.
2. **Frontal plane sampling:** the instantaneous solution is interpolated in a r, y planar grid of 0.1×0.1 mm immediately ahead of the detonation. To ensure that the plane never intersects the front, a constant forward shift of the mean angular position of the front in the direction of propagation is applied, i.e. the gas is sampled at the plane with $\theta_p(t) = \theta_m(t) + \Delta\vartheta$ with $\Delta\vartheta = 10$ deg.

The final output of the whole process is the series of instantaneous detonation front surfaces $\theta(r, y, t)$ and fluid properties $\varphi(r, y, \theta_p(t))$ on a moving plane directly before the detonation passage. The local instantaneous values of p, T and composition Y_k are also used as inputs for calculating the Chapman-Jouguet speed D_{CJ} through the Shock and Detonation Toolbox [46] based on the Cantera 2.4.0 [47] libraries for Python3.

It is worth noting that the mixture state in the frontal plane does not correspond exactly to the mixture which detonates, as $\theta(r, y, t) \neq \theta_p(t)$ and the detonation front requires a small but finite time interval $\Delta t = (\theta_p - \theta)/\omega_{det}$ to occupy the position of the sampling plane. However, the very high speed of the detonation front ($\omega_{det} \approx 47\,000\ rad/s$) and the small distance $\theta_p - \theta \approx 10\ deg$ between the detonation front $\theta(t)$ and the frontal plane $\theta_p(t)$ allows for neglecting the temporal variations of the flow within $t \pm \Delta t$ in a fixed point (r, y, ϑ):

$$\varphi(r, y, \vartheta, t) \approx \varphi\left(r, y, \vartheta, t \pm \frac{\theta_p - \theta}{\omega_{det}}\right) \tag{3}$$

With this assumption, the gas properties on the front can be obtained from the gas state recorded on the plane at a previous instant $t - \Delta t$, i.e. when the frontal plane occupied that angular position on the front:

$$\varphi\big(\theta(r, y, t)\big) \approx \varphi\left(r, y, \theta_p\left(t - \frac{\theta_p - \theta}{\omega_{det}}\right)\right) \tag{4}$$

Note that while it is assumed that $\Delta t = (\theta_p - \theta)/\omega_{det} \approx 0$, the correct spatial sampling at $\theta_p(t - \Delta t) = \theta(r, y, t)$ is preserved, retrieving the correct gas position with respect to the injectors. For these considerations, a single plane for sampling the state of the gas ahead of the front is used, allowing a consistent simplification of the procedure without compromising the accuracy of the analysis.

Once the instantaneous detonation front surfaces $\theta(r, y, t)$ have been collected, the absolute speed in every point of the front $D(r, y, t)$ can be evaluated by supposing that the front propagates along its local normal direction. The calculation of the velocity is carried out on a downsampled dataset ($\Delta t = 1.3 \times 10^{-7}$ s, 7.7 MHz) to reduce high-frequency noise. More details about this calculation can be found in the Appendix.

An important aspect to be considered is that the detonation speed is calculated in the global coordinate system and could generally deviate from the speed with respect to the reactants. However, the speed of the detonation is about 3–7 times the gas speed in the refill region, so in the analysis the front speed in the global system also represents the speed in the reactants within a good approximation.

4. Results

In this section the results of the simulation are reported and discussed, beginning with the validation of the model by comparison with available experimental data. Due to the non-premixed injection of the reactants, the analysis is focused on the detailed description of the local gas properties in the refill region, providing a complete characterisation of the mixture and explaining its connection with the dynamics of the injector. Thereafter, the speed of the leading shock is studied to clarify the correlation with the local mixture, including the front response to the periodic mixture variations induced by the discrete fuel injection.

4.1. Model validation

The harsh conditions typical of RDCs represent a great challenge for the diagnostics, so usually the measurements which can be carried out are limited. During the experimental testing of the rig, global features of the combustor such as the wave speed and number, the overall pressure gain and the pressure axial distribution were measured, and are adopted here as metrics to assess the accuracy of the numerical model.

4.1.1. Global flow field features

For the operating conditions considered in this study (Table 1), a dominant single detonation wave stabilizes in the chamber annulus. The simulation captures the same behaviour observed experimentally, with a single, well-defined front propagating in the combustor without major fluctuations. The presence of the detonation wave in the chamber partially blocks the effective injector area, leading to an inlet mass flow rate of 445 g/s (74% $\dot{m}_{is}$) for the air and 13.3 g/s (82% $\dot{m}_{is}$) for the fuel, targeting the nominal stoichiometric equivalence ratio.

The single detonation wave is clear from the shocks present in the combustor chamber (Fig. 4(a)) and the unwrapped temperature and hydrogen fields at mid-span (Fig. 4(b)). The detonation front exhibits a well-defined shape. Trailing the detonation is a strong

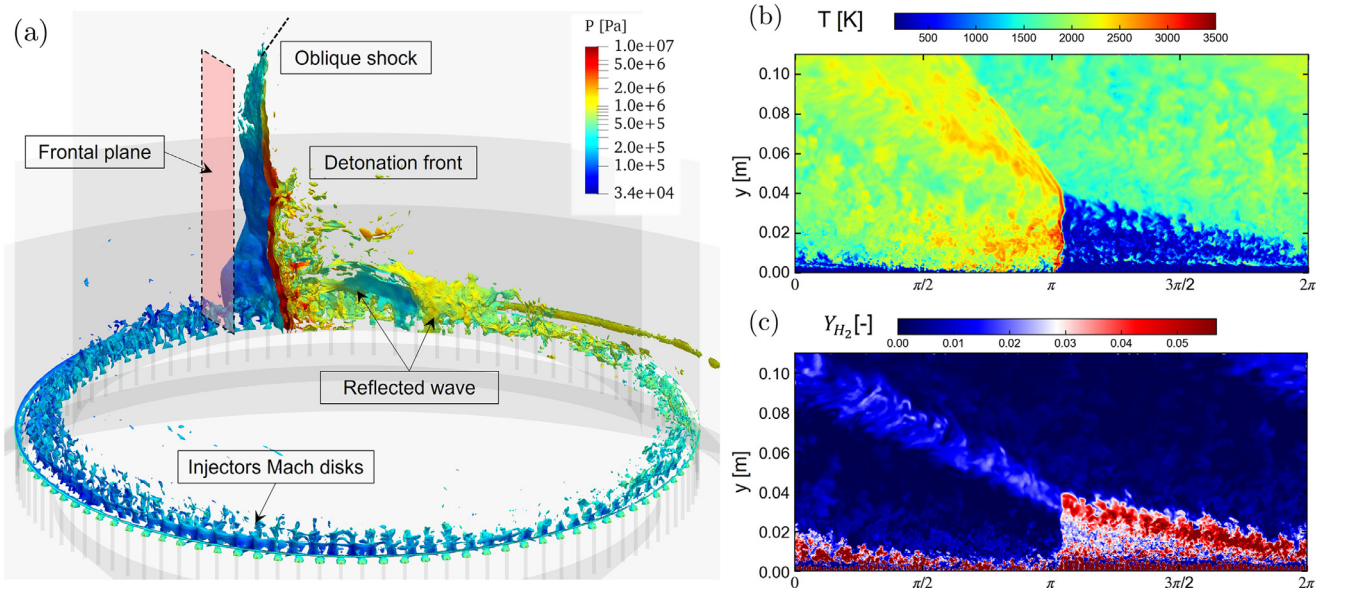

Fig. 4. Shock structures visualised through the $\nabla P/P = 2000\ m^{-1}$ isosurface and coloured by static pressure (a); maps of static temperature (b) and H_2 mass fraction (c) in the unwrapped mid-span cylindrical section of the chamber.

shock generated by the reflection of the detonation on the outer wall, typical of curved channels. This reflected shock wave persists for a relatively long azimuthal distance as it bounces off the inner wall, before returning to the outer radius and again blocking injectors.

Similarly to previous studies in other configurations [24], this trailing wave is not associated to an appreciate heat release as it mostly propagates in combustion products. Despite the high pressure obtained behind the detonation, no hot gas backflow is observed in the simulation in either of the injector channels.

The temperature and hydrogen mass fraction distributions resulting from the single wave are also reported in Fig. 4 at the midspan of the combustion chamber. The refill region begins approximately 60 *deg* behind the detonation wave and increases linearly up to a maximum refill height of approximately 40 mm. The hydrogen mass fraction field shows that the non-premixed injection results in large composition variations of the mixture ahead of the detonation front, even leading to a non-negligible 11% of the fuel mass flow rate exiting the combustor (1.46 g/s) unburnt. As the characterization of the gas mixture ahead of the detonation is of primary importance, it will be analysed in detail after presenting the model validation.

4.1.2. Wave rotation speed

During the experimental test, the pressure signals in the outer wall are measured using piezo-electric sensors at a frequency of 500 kHz [9]. The signals are sampled over several hundreds of milliseconds and then processed by fast Fourier transform, leading to a stable, average rotation frequency of 6287 ± 5 *Hz*.

Although the simulation enables more accurate and detailed procedures for determining the detonation speed, in this section the calculation is carried out by sampling several punctual probes distributed according to the real sensors in the rig. More specifically, the speed of the wave in the laboratory coordinate system is evaluated from the static pressure signals in different locations within the combustion chamber over 14 revolutions (≈ 1.8 ms). The probes are positioned at the chamber midspan with angular position $\vartheta = -20$, 33, 100, 220 *deg* for M6, M8, M9, M10, respectively. The signals are sampled with a frequency of 7.7 MHz at $y = 25$ mm and are reported in Fig. 5. The rotation speed $V = \omega r_{mean}$ is calculated from the time-of-flight between two adjacent pressure peaks $V = \Delta\vartheta r_{mean}/\Delta t$ either considering a single probe ($\Delta\vartheta = 2\pi$) or a consecutive pair, i.e. by considering the time interval between two adjacent stations. The wave predicted by the simulation propagates at the mean radius with an average speed of 1942 m/s (7509 Hz) with minor fluctuations of roughly ±26 m/s. Considering a CJ speed of 1975 m/s for H_2-air at stoichiometric conditions, the tangential velocity of the detonation is distributed around the Chapman-Jouguet value, resulting in a slightly under-driven condition along the inner wall and over-driven in the outer wall. The rotation frequency is overestimated by the simulation by 19% when compared to the value measured in the experimental test (1627 m/s, 6287 Hz), as reported in Table 3.

Table 3
Predicted and measured combustor characteristics.

		LES	Exp.
Wave type	[–]	Single	Single
Wave frequency	[Hz]	7509	6287
$V = \omega r_{mean}$	[m/s]	1942 (98% D_{CJ})	1627 (82% D_{CJ})
Exit total pressure $p_{0,e}$	[bar]	3.18	3.12
EAP_i	[bar]	3.17	–
EAP_i full	[bar]	3.33	–
Pressure gain PG	[–]	−0.57	−0.58

The reasons of the frequency overestimation still need to be clarified. Previous studies with realistic non-premixed configurations have observed both the overestimation [18,21,22,24] and underestimation [11,48] of the propagation speed with respect to the measurements. In the present analysis, the discrepancy could be primarily linked to the adiabatic treatment of the chamber walls, accordingly to what is observed by [18,21,22]. Moreover, the use of a combustion model that underestimates the deflagration speed could limit the proportion of burnt gas pockets in the refill region and partially avoid the wave weakening, as shown in other studies with considerable parasitic combustion [11,24,49]. Both of these two modeling aspects will be subject of further developments of the numerical model.

Although the simulation predicts a detonation frequency higher than the experiments, this difference is still reasonable and aligned with other works. Therefore, the flow field induced by the wave propagation as well as the reactants mixing are expected to be rea-

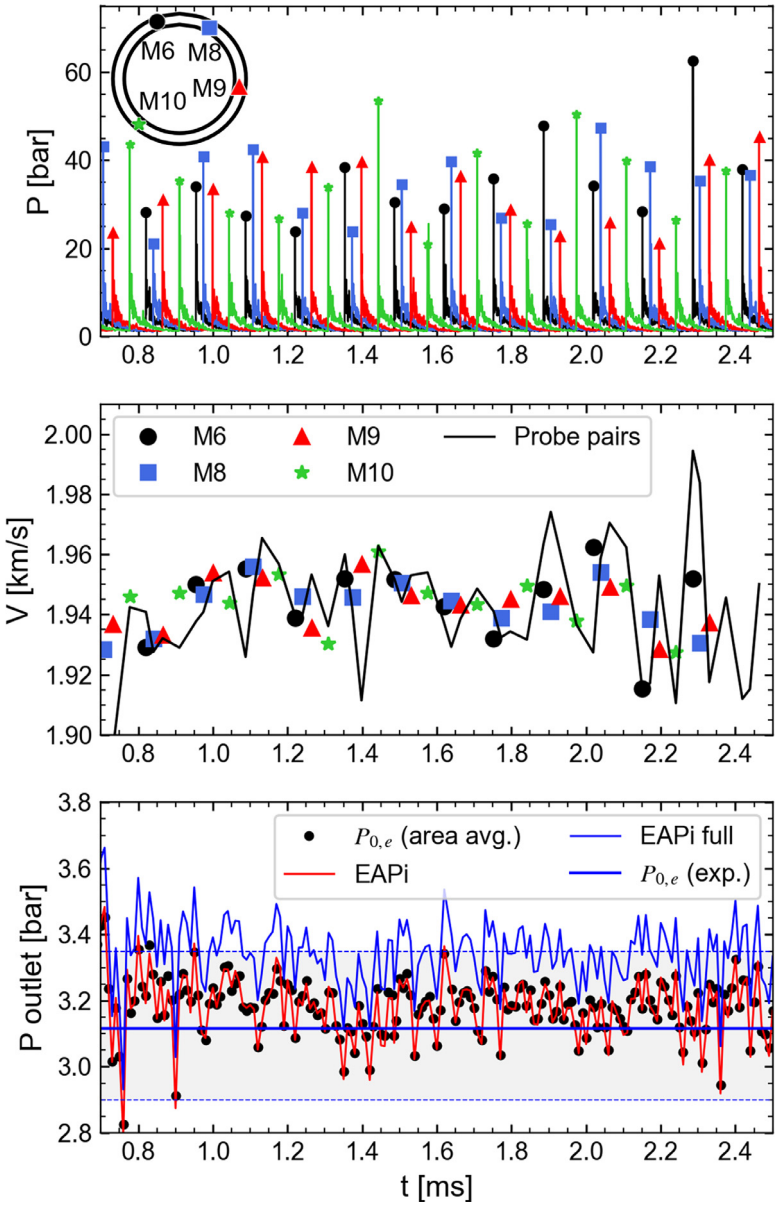

Fig. 5. Static pressure signals sampled at 7.7 MHz in four consecutive locations within the chamber at $y = 25$ mm and 50% span (top) and the resulting wave rotation speed (middle); instantaneous total pressures calculated at the outlet section. The grayed region indicates the average and RMS total pressure measured by Bach et al. [31] (bottom).

sonably representative of the real combustor operation with good approximation.

4.1.3. Pressure measurements

As reported in Table 3, the present configuration does not achieve a positive pressure gain, but rather it represents one of the most penalizing conditions for the combination of unrestricted outlet and relatively small air injector [9].

The total pressure at the RDC discharge measured with a Kiel probe recorded an average value of $P_{0,e} = 3.12$ bar for the present test conditions (Table 3). Considering the air plenum pressure of $P_{0,a} = 7.42$ bar, this leads to a negative pressure gain of $PG = P_{0,e}/P_{0,a} - 1 = -58\%$, primarily due to the high-loss injector. The overall pressure gain of the combustor is captured by the simulations with excellent accuracy (Table 3). The predicted area-averaged total pressure $P_{0,e}$ at the discharge is also reported in Fig. 5 (bottom) against the value measured by Bach et al. [31]. The agreement with the experiment in terms of overall pressure levels and gain, notwithstanding the wave frequency overestimation, seems to indicate that the detonation speed is not solely responsible the pressure gain, at least considering a single wave mode without outlet restrictions. A similar result was obtained by Sato et al. [22], where the pressure distribution in the experiments and in the simulations matched although the experimentally measured wave speed was lower. This behaviour is aligned to what is also seen in these measurements, such that other parameters are needed for characterising the performances of the combustor [9].

It is worth remarking that the experimental estimation of the effective pressure gain of RDCs is not trivial and a consolidated procedure must be still established. Since the combustor will be coupled with a downstream component – either a nozzle or a turbine – the pressure gain should consider the ability of the flow to produce the actual output of the engine [50]. To provide a more significant parameter, the ideal EAP is evaluated from the LES either by assuming the recovery of the axial flow velocity only (EAP_i) or all of the components (EAP_i^{full}). The values are reported in Fig. 5 (bottom) and Table 3.

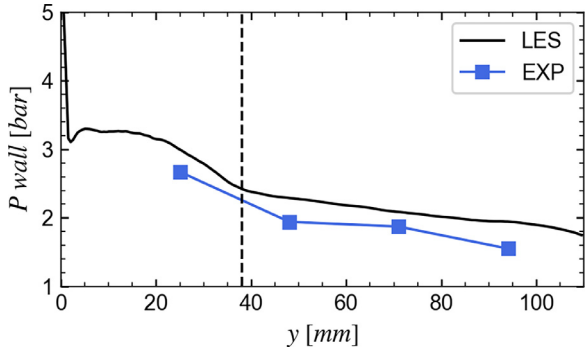

Fig. 6. Time-averaged axial distribution of the pressure along the chamber outer wall. The dashed line marks the refill height ($h \approx 38$ mm).

The temporal trends show that the EAP_i is coherent with the instantaneous total pressure at the outlet of the combustor, capturing not only the average value but also its fluctuations. This accordance is not surprising and was also observed in other studies which registered a limited difference between the two values [50,51]. As a consequence, the pressure gain is not affected by the choice of using EAP_i or the exit total pressure $p_{0,e}$, while the more optimistic value of EAP_i^{full}, including also the non-axial momentum, leads to slightly higher value (+2% increase). These observations suggest that the total pressure at the exit can be used as a meaningful value to evaluate the pressure gain of the device, thus supporting the approach carried out in the experiments [9,45,52].

Another important feature of the flow field inside the combustor to be predicted is the axial distribution of the pressure along the outer wall of the chamber. The time-averaged measurements of pressure in four different axial stations are reported in Fig. 6 and contrasted to the values calculated by the simulation. The profiles show a good agreement in terms of axial distribution, with different values depending on the relative position to the detonation wave. Below the refill height, the pressure is higher in the presence of the detonation, and then rapidly drops when the compression is provided only by the oblique shock. In this second region, the pressure decreases almost linearly toward the outlet.

The simulation slightly over-predicts the wall pressures as already observed in other studies [11,22], likely for the difference between the direct sampling in LES and the viscous attenuation of the experimental value for the Capillary Tube Average Pressure (CTAP) measure. Considering that the effects inside the capillary tube are not accounted for in the simulation, the comparison of Figs. 5 and 6 demonstrates a general accuracy of the pressure field.

The analyses carried out in this section support the model predictions as the pressure levels across the combustor appears to be well described. Therefore, there is no evidence that the error in the wave frequency invalidates the global flow field structure, such that the complex supersonic features present in the chamber are expected to be reasonably representative of the real RDC.

4.2. Refill region characterization

The time-averaged properties of the gas within the refill region in the radial-axial plane directly ahead of the detonation front (as described in Section 3.3) are reported in Fig. 7. The instantaneous samples are collected during a full wave rotation with a constant sampling rate, so they are evenly distributed with respect to the fuel injectors (see Fig. 4).

The refill region is evident from these maps and extends up to $h \approx 38$ mm from the chamber base ($Y_{H_2} < 0.015$). Since the time required by the wave to complete a revolution is around $\tau = 1.3 \times 10^{-4}$ s, the corresponding average axial velocity of the refilling mixture is around $h/\tau = 290$ m/s. The predicted refill height is in agreement with the nominal bulk flow value of $h = \tau \cdot \dot{m}/(\rho_u A_{cc}) = 36$ mm considering an ambient H_2−air stoichiometric mixture ($\rho_u = 0.855$ kg/m^3).

The average flow in the radial-axial plane immediately ahead of the detonation is completely driven by the non-premixed injection of the reactants, with the radial-inward air flow deflecting the axial fuel jet toward the inner wall of the chamber (Fig. 7(a)). Despite the higher mass flow rate, the supersonic jets are qualitatively similar to the results obtained by Weiss et al. [29] in non-reactive conditions. As a result of the deflection, the stirred reactants impinge on the centerbody deviating from a 45 deg angle to the axial direction. This flow curvature is allowed by the subsonic speed of the mixture and induces the formation of a high pressure region in the inner corner of the chamber. The average axial flow along the inner wall is slightly supersonic, but it is determined by averaging subsonic and supersonic gas pockets between $M = 0.7$–1.8. On the other hand, in the outer half span of the chamber the speed is subsonic, mainly due to the higher sound speed in this region rather than a reduction of the flow velocity. Above the reactant jets ($y \geq 5\,mm$) the static pressure field is relatively constant ranging between 1–1.3 bar, leading to an average total pressure in the refill region ahead of the detonation of $p_{0,ref} = 1.93$ bar. This value shows that a significant pressure drop occurs across the air injector ($p_{0,ref}/p_{0,a} = 0.26$), but also that an ideal pressure increase of roughly $p_{0,e}/p_{0,ref} = 1.65$ could be achieved neglecting the injector losses.

An important characteristic of the air radial injection is the formation of a recirculation region above the air gap in the outer wall. This region is constantly filled with hot combustion products (Fig. 7(b)-(c)) and promotes the parasitic combustion near the outer annulus wall. Indeed, the present injector configuration combined with relatively high mass flow rate allows an efficient refill in the inner half of the chamber only, flushing away the combustion products, while it is deficient for spans greater than 50%.

Although the inner half of the chamber is mostly fresh gas, the mixture is not homogeneous and presents a significant axial stratification (Fig. 7(d)). To better characterise the mixture and distinguish between stirred and mixed reactants, the fuel unmixedness [29,53]:

$$U_{H_2} = \frac{\overline{Y''^2_{H_2}}}{\overline{Y}_{H_2}(1-\overline{Y}_{H_2})} \tag{5}$$

is often determined from the fuel variance $\overline{Y''^2_{H_2}}$ as a metric for mixture quality, so it is calculated in the plane and reported in Fig. 7(e).

Three different zones can be identified in the fresh gas below the 50% of the span. At the top of the refill region, a wide pocket of rich, well-mixed reactants (1) extends for approximately a third of the total height (between axial positions 25 and 38 mm), featuring an equivalence ratio of $\phi = 1.13$–1.36. Below, a slightly lean and uniform mixture with $\phi \approx 0.85$ is present at the center of the refill zone (2). Near the chamber head ($y < 10$ mm) the gas composition fluctuates considerably due to the presence of the unmixed hydrogen jets (3) just entering the chamber. Here, the flow field is divided by the presence of the supersonic air flow and its interaction with the axial fuel jet, determining a fuel accumulation at the base.

This peculiar mixture stratification and its formation can be explained by considering the differential interaction between the high-pressure wave and the distinct reactant injectors. In fact, due to the different geometry, feeding pressure, and fluid within the air and fuel channels, their dynamics are different and are affected differently by the detonation blockage. Since the combustor oper-

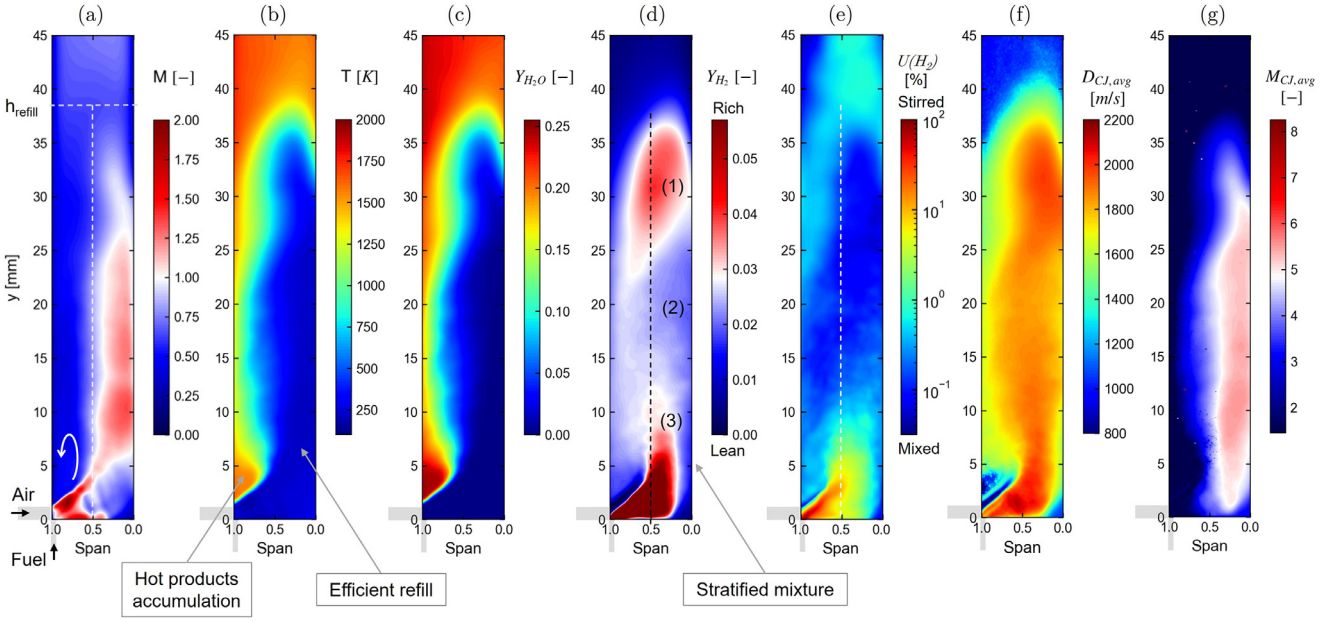

Fig. 7. Time-averaged gas properties of the refill region in the plane ahead of the detonation front ($\Delta\vartheta \approx +10$ deg), including the corresponding time-averaged local CJ speed and CJ Mach number in the fresh gas. The divergent maps of hydrogen (d) and M_{CJ} (g) are centred on the stoichiometric composition in absence of H_2O and the nominal CJ Mach number of 4.85 for a stoichiometric H_2-air detonation, respectively.

ates nominally at a stoichiometric condition, any local alteration to the fuel and air mass flow rates into the combustor produces regions that deviate from $\phi = 1$.

To characterise quantitatively the local departure from the nominal stoichiometric condition, polar diagrams of the instantaneous reactants mass flux and the resulting local air-to-fuel mass ratio (AFR) are reported in Fig. 8. The mass fluxes are normalized with respect to the value before the detonation passage ($\dot{m}_{0,a} = 1274\ kg/m^2s$ and $\dot{m}_{0,f} = 711\ kg/m^2s$) and highlight distinct phases of the injectors after the wave passage.

The minimum in reactant flow occurs roughly 10 *deg* behind the front and occurs in both the fuel and air at the same time. The injectors then starts recovering until the reflected wave again perturbs the flow about 60 *deg* behind the detonation, with about half the intensity of the first blockage. The combined effect of these two waves results in an severe perturbation of the injectors during the first 90–120 *deg* behind the front.

Despite the simultaneous blockage, the air mass flux is reduced considerably more than the fuel mass flux due to the differing injector pressures, resulting in a local low value of *AFR* and an excess of injected fuel mass in the 30 *deg* behind the front. Around 40 *deg*, the air flow recovery results in a local $AFR \approx 34$ ($\phi \approx 1$), but then the second blockage lowers again the *AFR* at 60–75 *deg*. This behaviour of the injectors produces first a gas entering in the chamber within 0–75 *deg* with a fuel-rich composition, which then mixes while being advected downstream by the following reactants, settling at the top (1) of the refill region (Fig. 7). Due to its position, this region is particularly detrimental to the combustor operation as the lack of oxidizer leads to a significant proportion of unburnt hydrogen exiting the chamber (11% of mass), visible in Fig. 4.

After the second blockage, the fuel mass flow rate rapidly stabilizes to the unperturbed values ($\vartheta \geq 90\,deg$), while the air requires an additional 30–40 *deg*. However, while the fuel mass flow rate reaches the choking value, the air mass flow rate exhibits its maximum value between 120 and 270 *deg*, inducing a slightly lean reactants ratio with $\phi = 0.85$. Only after 270 *deg* behind the detonation does the air mass flux decreases again, finally matching the nominal stoichiometric ratio.

This particular phenomenon can be regarded as a consequence of the moving shock passage inside the air gap and propagating upstream toward the plenum. Since the moving shock temporarily induces a total pressure increase, between 90 and 270 *deg* the local total pressure at the end of the air gap is slightly higher, so the fluid is more dense at the throat and the choking mass flow rate is increased. This effect progressively decreases with the distance from the shock within the airgap, until at $\vartheta = 270$ *deg* the temporary total pressure rise is not relevant, leading to a reduction of mass flow rate.

Secondarily, the air excess could be linked to a local variation of the air throat area. In the present configuration, the fuel throat area is determined uniquely by the geometry, while the air throat area also depends on the shape of the fuel jets, which reduces the geometric area of the air gap. Although the choking air mass flow rate could be potentially influenced by the fuel blockage, no significant differences in the air throat were observed between 180 and 320 *deg* analysing the $M = 1$ isosurface.

The three injector phases described above result in the axial stratification of the mixture shown in Fig. 7(d). The analysis carried out in this section confirms that the detonation and reflected wave have a significant impact on the injectors, resulting in significant inhomogeneities in the fresh mixture as a consequence of the different, uncontrolled alteration of fuel and air mass flow rates. Indeed, these are undesired features for the RDC, so the effects of the reflected shock should be carefully taken into account when optimizing the combustor operation. More specifically, the axial stratification of the fresh mixture could be reduced by a re-design of the injectors considering the following points:

- The differential effects of the detonation blockage on the air and fuel injectors result a rich region at the top of the refill region, so an optimized geometry should try to minimize or equalize the transient response of fuel and air to maintain the equivalence ratio;
- The moving shock propagating upstream in the air injector locally increases the total pressure, increasing the local mass flow rate, thus the injectors geometry should avoid or dissipate the propagation of the shock.

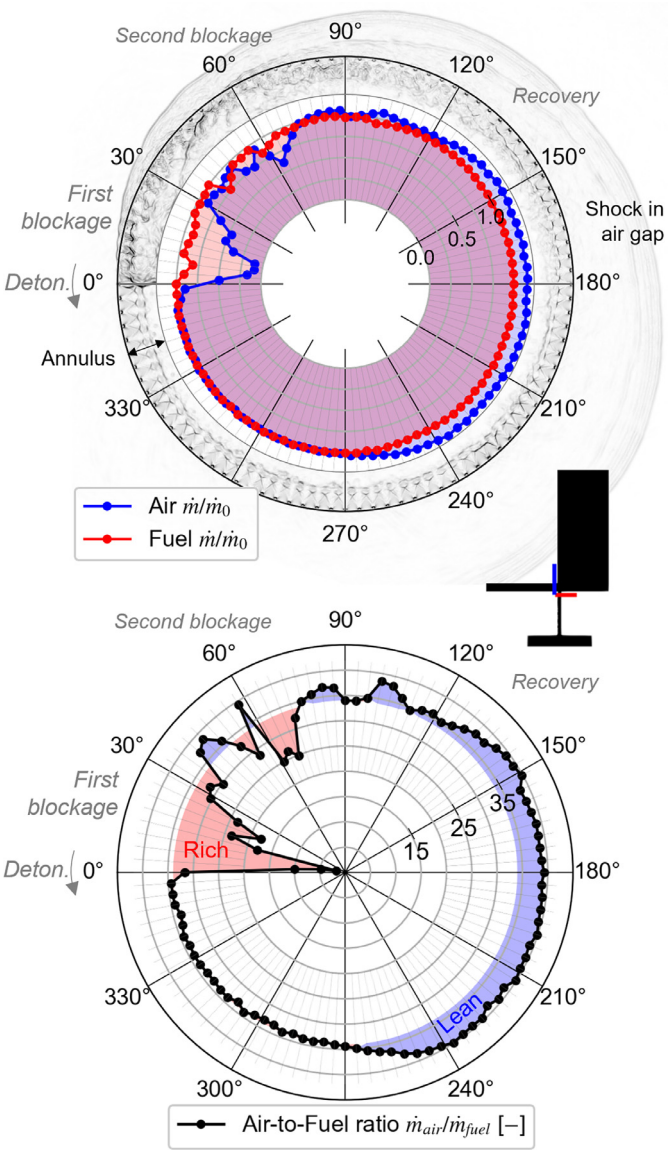

Fig. 8. Polar diagrams of the local instantaneous mass flux at the injectors exit superimposed on the numerical schlieren at the chamber base (top) and the resulting Air-to-Fuel ratio (AFR, bottom) with respect to the nominal stoichiometric value ($AFR = 34$). The detonation is located at $\vartheta = 0$ *deg* and the mass fluxes are normalized with the value before the detonation passage.

4.2.1. Local Chapman-Jouguet speed

The knowledge of the instantaneous local gas state ahead of the detonation front allows for the calculation of the local Chapman-Jouguet speed in the plane. The instantaneous distributions of the CJ speed are then time-averaged and the result is reported in Fig. 7(f). Equivalently, also the CJ Mach number in the fresh mixture $M_{CJ} = D_{CJ}/a_0$ is evaluated and time-averaged in Fig. 7(e).

As the detonation speed depends most strongly on the equivalence ratio, the average D_{CJ} is higher in the rich regions below the fuel jet and in the top part of the refill region, while it decreases toward the outer wall due to both the leaner composition and the higher temperature residual products. Due to the high variability of the composition at the chamber base, the RMS of the CJ speed (not reported) reaches its maximum values of 500 m/s, while is generally limited below 150 m/s in the other regions.

The recirculation region above the air gap features values of D_{CJ} near the local sound speed which is already high due to the presence of hot products, as clear from the M_{CJ} distribution with values approaching 1 around $y = 3$ *mm* on the outer wall. Such low M_{CJ} are unlikely to be able to self-support the detonation in this region, and therefore the wave propagation in this region is likely supported by the stronger neighboring regions in the annulus. At the top of the refill region, the more intense deflagration vitiates the reactants near the outer wall, broadening the low CJ speed layer present at high span. The mixture properties alone would then induce a slower propagation along the outer wall with respect to the inner wall, which is in opposition to what is observed here (see Section 4.3) and typically in curved channels [54] and other RDC studies [16].

The CJ speed distribution in Fig. 7(f) remarks that in a non-premixed combustor the mixture properties can deviate significantly from an ideal premixed case at the same conditions. For instance, the mean CJ speed between $5 < y < 35$ *mm* is 1807 m/s, much lower than the reference of 1975 m/s at ambient stoichiometric conditions.

The local values of CJ speed are particularly interesting as they describe the speed at which a steady, unperturbed detonation should propagate in the local mixture. Therefore, the discrepancy between the actual front speed and the CJ speed should be attributable to missing effects in the CJ theory such as wave unsteadiness and annulus curvature. The comparison between the two will be presented in Section 4.3.

4.2.2. Periodic gas variation for the discrete injection

The quantities on the frontal plane exhibit periodic fluctuations forced by the presence of the discrete fuel injectors, but which are also affected by turbulence. For describing the periodic deterministic component of the quantities without the spurious contribution of the instantaneous turbulence, the instantaneous gas properties ahead of the front are Phase-Locked Ensemble Averaged (PLEA) according to [55,56]:

$$\varphi_{\text{per}}(r, y, \Theta_p) = \frac{1}{N}\sum_{k=0}^{N-1} \varphi\left(r, y, (\Theta_p + k)\Delta\theta_{inj}\right) \tag{6}$$

where $k \in \mathbb{N}[0, N-1]$, N is the number of injectors and $0 \leq \Theta_p < 1$ is the phase relative to the fuel injector, such that any frontal plane position can be expressed as $\theta_p = (\Theta_p + k)\Delta\theta_{inj}$. Since the data is sampled for discrete values of Θ_p, the phase space is divided into 20 bands of width $\Delta\Theta_p = 0.05$, centred around Θ_p.

The PLEA fields of hydrogen mass fraction and local CJ speed are averaged in the radial direction and reported in Fig. 9 in the injector phase space.

The map does not show a noticeable variation with the phase, except for the unavoidable fluctuation in region (3) below $y = 10$ *mm*, that directly involves the fuel jets. Downstream, the PLEA axial values coincide with the time-average as soon as the reactants jets start mixing. This feature demonstrates that for this combustor configuration, the fuel injectors (100×0.5 *mm*) are dense enough to determine a tangentially uniform mixture, mostly independent of the discrete hydrogen jets. The well-mixed reactants in regions (1) and (2), with a constant composition during the wave rotation, promote a steady stabilization of the wave. This however may not be representative for other configurations with a longer fuel injector pitch.

An interesting aspect that emerges from the PLEA maps in Fig. 9 is that the periodic variations at the chamber base (3) is not perfectly symmetric, i.e. they are not symmetric around the plane in-between two injectors $\Theta_p = 0.5$, but exhibit a phase shift of $\Delta\Theta_p \approx -0.05$. This behaviour is observed between $\Theta_p = 0.2$–0.8, where the gas between two injectors is always slightly richer near the injector in the direction of the detonation propagation ($\Theta_p > 0.5$) than near the other one at $\Theta_p < 0.5$. The shift is attributed to the tangential velocity induced by the detonation in the

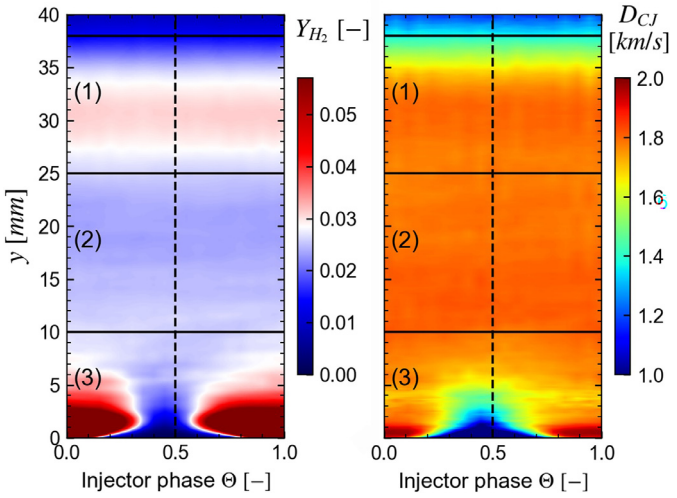

Fig. 9. Phase-Locked Ensemble Averaged axial distributions of hydrogen mass fraction (left) and CJ speed (right) in the frontal plane, averaged in the radial direction. The vertical dashed line indicates the injector phase in-between two injectors ($\Theta = 0.5$), while $\Theta = 0,\ 1$ correspond to the injector axis. The detonation wave moves from $\Theta = 0$ to $\Theta = 1$.

refill region, which slightly deflects the fuel jets in the opposite direction with respect to the wave, i.e. $-\Theta$. In other words, the minimum fuel concentration is not occurring, as expected, in-between two fuel injectors, but has a small shift.

The mixture composition directly impacts the CJ speed (Fig. 9, right), however, the radial average above the jets in regions (1) and (2) presents a nearly uniform value around 1750–1800 m/s. However, at the base of the chamber in region (3), the succession of pure hydrogen and air streams periodically decreases the CJ speed as the mixture exits the detonability limits. As the wave speed dependence on transversal composition gradients has been observed both experimentally [57] and numerically [11,49], the region (3) could reduce the stability of the front by inducing periodic fluctuations in the order of 750 kHz.

The PLEA fields of the other gas properties exhibit phase distributions similar to Fig. 9, so they are not reported for sake of conciseness.

4.3. Detonation front topology and speed

The detonation front that stabilizes in the chamber annulus presents a defined three-dimensional shape throughout the revolution. Considering a cartesian coordinate system (d, r, y) rotating around the combustor axis which follows the average angular position of the front $\theta_m(t)$, the detonation surface can described by the linear distance of the front from a radial-axial plane passing through its center $\theta_m(t)$:

$$d(\theta, \theta_m) = d(r, y, t) = r \sin\left(\theta(r, y, t) - \theta_m(t)\right) \tag{7}$$

The time-averaged maps of front elevation are reported in Fig. 10(a). The peculiar feature of the front is the presence of an almost conical protrusion along the outer wall with the vertex positioned above the air gap edge. This structure presents continuous and wide azimuthal fluctuations in contrast to the other parts of the front which exhibit weaker variations. From the maps, this protrusion is clearly visible with the vertex positioned around $y = 2$ mm on the outer wall and the semi-circular base between the air gap edge and about $y = 10$ mm, surrounding the recirculation region shown in Fig. 7.

The regions around the inner corner of the chamber, however, exhibit a good stability and are nearly flat or slightly recessed with respect to the majority of the front. While a clear correlation between the surface shape and the gas state in the frontal plane is not observed, the most protruding regions appear to be positioned in correspondence to regions of a high temperature and sound speed. A similar feature was described also in other RDC configurations and linked to the higher local sound speed [24], indicating that these regions are then supported by the core of the detonation within the more stable region (2).

It is worth highlighting that no clear detonation cells are observed from the analysis of the instantaneous front surface, but rather only small-scale front fluctuations related to the fresh gas turbulent conditions are present.

The time-averaged normal velocity of the front D is also reported in Fig. 10(b), as well as its ratio to the local D_{CJ} to highlight the over-driven and under-driven regions (Fig. 10(c)). The average radial profiles far from the injection ($10 < y < 35$ mm) are also represented in Fig. 11.

The region (3) near the chamber base ($y < 10$ mm) needs a specific discussion since here the speed is influenced by the continuous fragmentation of the front due to the presence of the supersonic reactants. The part of the protrusion which exhibits the higher stability is the peak at $y = 3$ mm along the outer wall and always constitutes the leading point of the front. The propagation of this portion occurs at speeds of 1900–2000 m/s, consistent with the other parts of the front, but not with the local CJ speed, which approaches the local sound speed. The wave in the recirculation above the air gap is thus likely supported by the neighboring regions which are detonating.

In the stable part of the front, in regions (1) and (2) (i.e. $y >$ 10 mm), the detonation speed shows a linear increase from the inner to the outer wall. This variation does not appear directly determined by the mixture properties in the refill region (Fig. 7), i.e. by the local CJ speed. This observation holds also for the rich region at the top of the refill height (1), which does not noticeably affect the detonation speed of the front.

Rather, the detonation velocity is distributed around the local CJ speed, so that the regions adjacent to the inner wall are slightly below D_{CJ} (-5%), while at spans above 50% it is increasingly overdriven up to $+20\% D_{CJ}$ (Figs. 10(c) and 11). This is partially due to the lower CJ speed near the outer wall (Fig. 7), with the absolute front speed raising up to 2000 m/s at the outer wall compared to 1800 m/s along the inner wall. Globally, the majority of the front with a flammable mixture propagates between $\pm 5\% D_{CJ}$. The overdriven speed at the outer wall is consistent to what usually observed in curved channels and premixed reactants, i.e. with uniform local CJ speed [16,54].

Indeed, the difference between the actual front speed and the CJ value could be attributed to effects not included in the CJ theory, as the wave unsteadiness, mixture stratification and annulus curvature. The average front velocity shows a balance between the effects of the local mixture distribution and the curvature effects at the outer and inner walls. The reduction in the propagation velocity due to the dis-homogeneity of mixture properties, resulting in the reduction of expected CJ properties, is overcome by the compressive effect of the outer wall, having the net effect of an increase in the effective wave speed with the radius. The opposite effect is observed along the inner wall. The balance of these effects may help to explain the experimental observation that, as the reactant flow rate decreases for a given nominal equivalence ratio, the wave speed decreases until failure. These results indicate that this failure may be the result of the shifting in the balance, whereby the weakening of the compressive effect can no longer overcome the low-quality mixture along the outer wall resulting in an increasing disparity in normal velocity across the span and the ultimate wave failure.

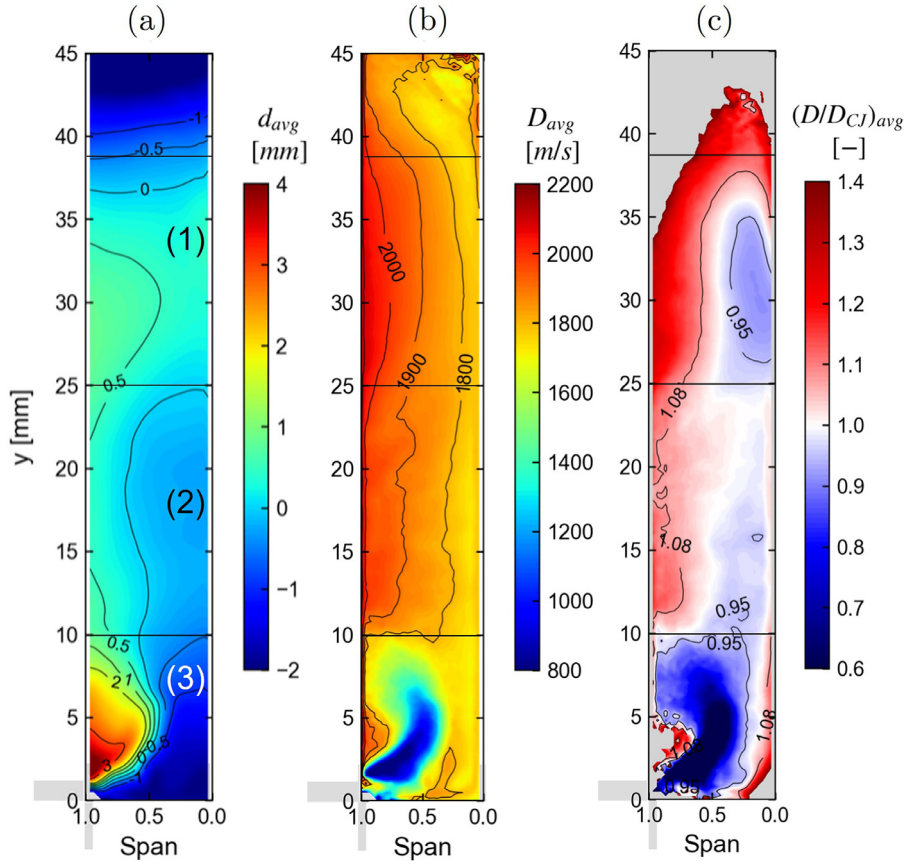

Fig. 10. Time-averaged radial-axial maps of the detonation front elevation (a), speed (b) and ratio of the front speed to the local CJ speed (c). The horizontal lines mark the regions (1)-(3).

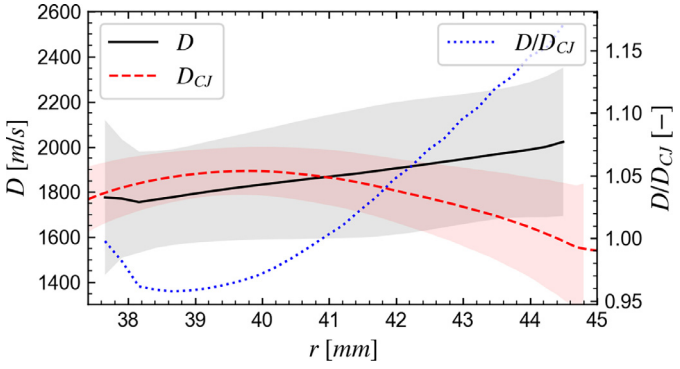

Fig. 11. Time-averaged radial distribution of the detonation speed between $10 < y < 35$ *mm* with the respective local RMS represented by the colored area.

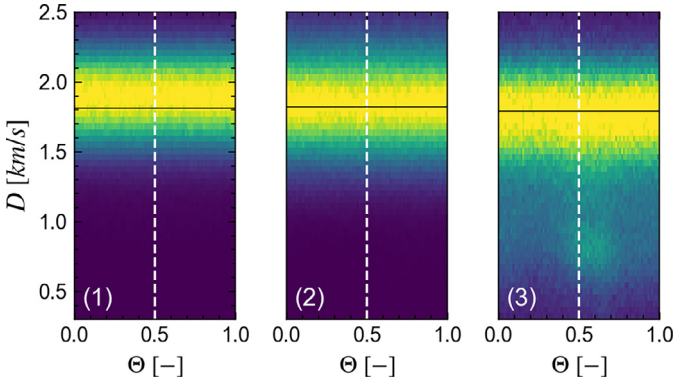

Fig. 12. Two-dimensional PDFs of the local detonation front speed in the injector phase space in the axial regions (1): $25 < y < 35$ *mm*, (2): $10 < y < 25$ *mm*, (3): $0 < y < 10$ *mm*. The dashed line marks $\Theta = 0.5$ and the horizontal lines the time-averaged CJ speed in each reagion.

4.3.1. Injector-induced tangential fluctuations

As discussed previously, the refilled gas ahead of the front exhibits a variation in the discrete fuel injection only at the chamber base ($y < 10$ *mm*), inducing important fluctuations of the local CJ speed (Fig. 9). It is then interesting to assess whether the front propagates either according to the unsteady region (3) or to the more uniform regions (1) and (2). To investigate and highlight any statistical dependence of the local the propagation speed on the front position with respect to the fuel injectors, the instantaneous speed values can be represented in the injector phase space Θ (see Section 4.2.2). The two-dimensional Probability Density Functions (PDF) of the detonation speed at each instant and point in the front for the three main regions identified in Fig. 9 are reported in Fig. 12.

Far from the injection, i.e. in regions (1) and (2), the wave speed does not show any statistical dependence on the injector phase, even at the middle of the gap between the fuel channels ($\Theta = 0.5$). The velocity at each position is distributed around a constant average which is not far from with the local D_{CJ}.

On the other hand, the near-injection region (3) not only features a wider deviation toward lower values from the average CJ speed, but also non-negligible eventual speed reductions in-between the jets (Fig. 12, bottom). In fact, distinct speed drop events are also present between the injectors at $\Theta \approx 0.6$, highlighting that a temporary, local deceleration of the leading shock has

higher probability to occur between the fuel jets. The region interested by this phenomenon corresponds only to the low CJ speed zone in Fig. 10(c). This observation confirms that the periodic CJ speed reduction in Fig. 9 around $\Theta = 0.45$ has an impact on the detonation speed, but the response of the front is slightly delayed of $\Delta\Theta = 0.15$, i.e. $+0.54$ *deg* in the propagation direction. In other words, although the CJ theory is not able to represent completely the complex propagation of the wave, a temporarily, local variation of the detonation speed is likely to occur right after a pocket of pure air, where the CJ speed is low or not defined. It is also worth to remark that this is a stochastic behaviour and is not occurring at the passage frequency of the injectors of about 750 *kHz*.

In conclusion, the PDFs maps reported in Fig. 12 show that the fluctuation of CJ speed has only a local and sporadic impact on the wave speed, so the front at the base of the chamber is likely to have a secondary importance for the stability of the whole wave, which propagates steadily during the rotation. Therefore, the central region of the refill region appears to be the most important region for the stabilization of the detonation.

5. Conclusions

The non-premixed Rotating Detonation Combustor (RDC) installed at TU Berlin is numerically investigated by means of fully-compressible, multispecies, reactive Large Eddy Simulations with the AVBP code. The high temporal and spatial resolution of the simulation allowed the detailed description of critical aspects of the combustor operation, such as the wave-injector interaction, the refilled gas properties and the front propagation speed.

The main outcomes of the work can be summarised as follows:

- According to the experimental observations, a single wave establishes in the combustor and propagates steadily at 7509 *Hz*, over-estimating the recorded frequency by +19%. Nevertheless, the axial pressure distribution and overall pressure gain of the device are well captured by the simulation, with the exit total pressure matching the measurements.
- As a consequence of the radial-inward air injection and the high mass flow rate, only the refill region within 50% span is efficiently flushed with fresh reactants, while the outer half of the refill region contains a large proportion of residual hot products.
- The gas ahead of the detonation front presents consistent variations both in radial and axial directions, with a rich region at the top of the refill height, a slightly lean central region and unmixed reactants at the chamber base. This axial stratification is due to the differential blockage and recovery of the fuel and air injectors and could be avoided by modifying the injection system to minimize or equalize the dynamics of the injectors ducts.
- The average front velocity is the result of the balance between the effects of the local mixture distribution and the curvature effects at the outer and inner walls. Although the wave speed is mostly distributed around the local CJ speed ($\pm 5\%$), near the outer wall the low-quality of the mixture is overcome by the compressive effect of the wall, determining an increase of speed at high radii.
- Notwithstanding the periodic variation of the refilled mixture near the chamber base due to the presence of the discrete fuel injectors, the global detonation speed does not show corresponding high-frequency fluctuations. Only near the reactants jets, where the local CJ speed is lower due to the presence of the supersonic air flow, the wave speed has a higher probability to exhibit temporary velocity drops.

This study demonstrates how the complete resolution of the injection system is fundamental to capture the interaction between the waves and the reactants. Deeper understanding of the injectors operation is indeed an essential aspect for the optimization of the RDC performances, since it not only drives the mixture preparation, but also the overall combustion efficiency and pressure gain which can be achieved. In this context, the present study represents a first step for characterizing the main aspects related to the RDC operations and provides valuable insights for the future design improvements.

Declaration of Competing Interest

The authors declare that they have no known competing financial interests or personal relationships that could have appeared to influence the work reported in this paper.

Acknowledgments

Research carried out in the Italian National Recovery and Resilience Plan (NRRP), funded by the European Union – NextGenerationEU. Award Number: Project code CN_00000023 Italian Ministry of University and Research, Project title “Sustainable Mobility Center – Spoke 12”. The authors would like to acknowledge Dr. O. Dounia, Dr. N. Odier and E. Bach for the useful discussions and CERFACS for the grant to use the AVBP code.

Appendix A

Detonation speed calculation

The detonation front speed in the global system can be evaluated from the time series of the surfaces $\theta(r, y, t)$ by supposing that the front propagates along its local normal direction $\underline{n}$. The unit normal of the front is computed from the surface $\theta(r, y, t)$ expressed in a cartesian coordinate system (d, r, y) rotating with the average angular position of the front $\theta_m(t)$ (Fig. A.1).

In such space, the detonation front surface is described by the function:

$$d(\theta, \theta_m) = d(r, y, t) = r \sin\left(\theta(r, y, t) - \theta_m(t)\right) \tag{A.1}$$

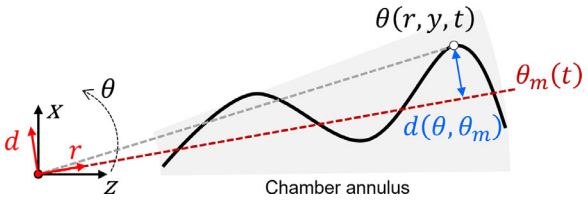

Fig. A.1. Representation of the reference frames adopted for describing the detonation front (black line). (x, y, z): global cartesian system, (ϑ, r, y): global cylindrical system, (d, r, y): cartesian system rotating with the front.

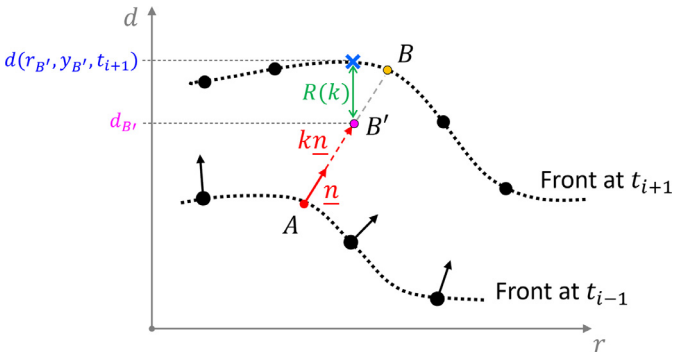

Fig. A.2. Determination of the front normal displacement.

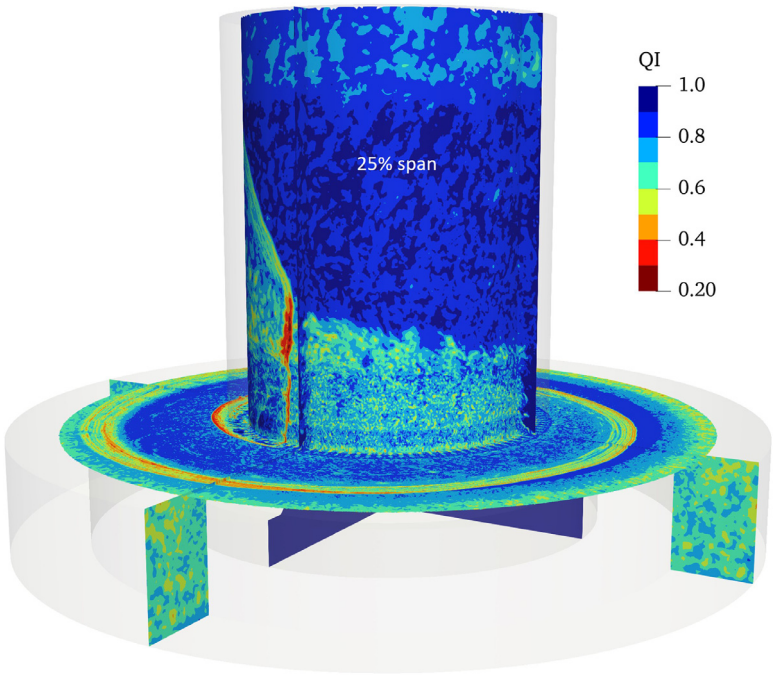

Fig. A.3. Instantaneous fields of Celik's LES quality index.

which can be reformulated in its implicit form $F = f - d(r, y, t) = 0$ and spatially derived to obtain the unit normal vector:

$$\nabla \mathrm{F} = \left(1, -\frac{\partial d}{\partial r}, -\frac{\partial d}{\partial y}\right) \tag{A.2}$$

$$\underline{n}(r, y, t) = \frac{\nabla \mathrm{F}}{|\nabla \mathrm{F}|} = \left(n_d, n_r, n_y\right) \tag{A.3}$$

The detonation speed at time t_i is then calculated from the displacement of the front along the local normal direction as the distance between the points $B(r, y, t_{i+1})$ and $A(r, y, t_{i-1})$:

$$(B - A) = k\underline{n} \tag{A.4}$$

The coordinates d of the points A and B in Fig. A.2 are both evaluated with respect to the same angular position $\theta_m(t_i)$, according to Eq. (A.1).

The calculation of the distance $|B - A|$ requires the B point position (d_B, r_B, y_B) on the detonation front, which is unknown since the surface describing the front is discrete, imposing the B point to be determined iteratively. This is done by considering a test point B' and equalling its coordinates $d_{B'}$ to the d coordinate of the point on the front at t_{i+1} interpolated on the B' coordinates (see blue cross in Fig. A.2):

$$d(r_{B'}, y_{B'}, t_{i+1}) = d_{B'} \tag{A.5}$$

When this occurs, also $B \equiv B'$ and the intersection condition is met. Considering also that:

$$\begin{pmatrix} d_{B'} \\ r_{B'} \\ y_{B'} \end{pmatrix} - \begin{pmatrix} d_A \\ r_A \\ y_A \end{pmatrix} = k \begin{pmatrix} n_d \\ n_r \\ n_y \end{pmatrix} \tag{A.6}$$

the following parametric function of k can be obtained:

$$d\left(kn_r + r_A, kn_y + y_A, t_{i+1}\right) = kn_d + d_A \tag{A.7}$$

The normal distance is then evaluated as the root of the residual $R(k)$:

$$R(k) = d\left(kn_r + r_A, kn_y + y_A, t_{i+1}\right) - kn_d - d_A \tag{A.8}$$

using the modified Powell method in Python. The root k represents the scaling factor of the unit normal $\underline{n}$ to intersect the front at t_{i+1}, i.e. $B' \equiv B$, so its value coincides with the displacement $|B - A| = k$. This procedure is carried out for each point (r, y) of the front and instant t_i, leading to the local instantaneous normal speed of the detonation $\vec{D}$:

$$\vec{D} = D(r, y, t_i)\underline{n} = \left(\frac{k(r, y, t_i)}{t_{i+1} - t_{i-1}}\right)\underline{n} \tag{A.9}$$

A preliminary application of the procedure using the sampling interval of $\Delta t = 3.25 \times 10^{-8}$ s (31 MHz) showed a high-frequency noise affecting the velocity. This was attributed to the excessive sampling rate which is comparable or lower than the time to flow through a mesh element (8.5×10^{-8} s in the refined region and 2.25×10^{-7} s in the chamber). Therefore, only for the velocity calculation, the data is downsampled by 4 times ($\Delta t = 1.3 \times 10^{-7}$ s, 7.7 MHz), filtering out the high-frequency fluctuations and improving the quality of the resulting velocity.

Assessment of the mesh grid effect

Additional information about the mesh resolution and impact on the solution is provided in this section. Since the effect of the mesh on the RDC is twofold, potentially involving coupled effects on both the turbulent mixing and the detonation front propagation, the two contributions are analyzed separately in the next.

As an index of the turbulent fluctuations resolution, the Celik's quality criterion based on the viscosity QI_ν is calculated as [40]:

$$QI_\nu = \frac{1}{1 + 0.05\left(\frac{\mu_{sgs}}{\mu}\right)^{0.53}} \tag{A.10}$$

The resulting values are reported in Fig. A.3. In the refill region the turbulent fluctuations, lead to values between $0.7 - 0.9$, with a slightly lower quality outside the refinement region at the base of the chamber. In the rest of the chamber, the acceleration of the burnt gases is associated to a high index quality $(0.8 - 1)$, notwithstanding the coarser mesh size. The most demanding region in

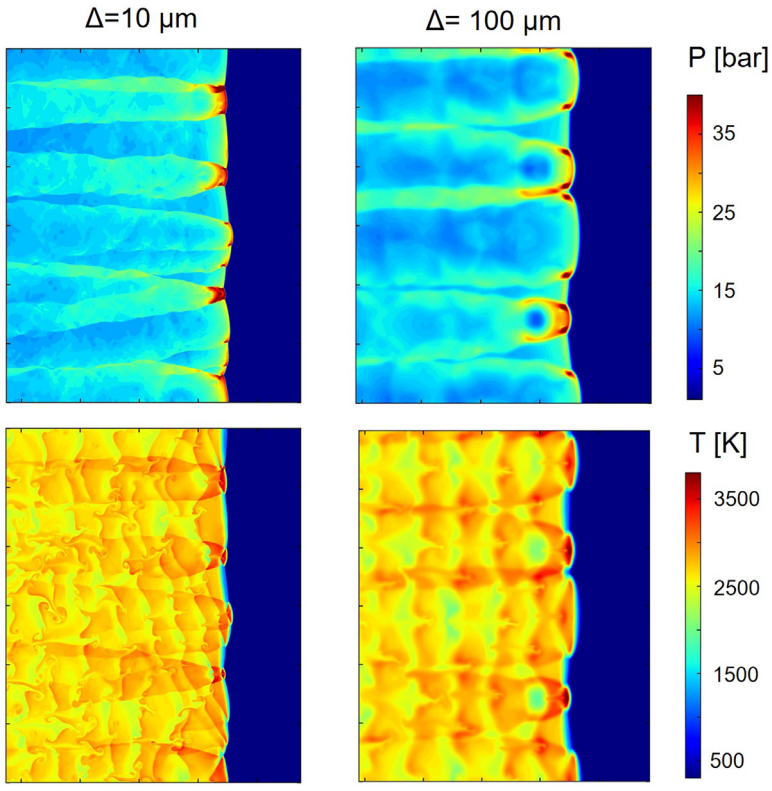

Fig. A.4. Instantaneous detonation front in a 2D detonation channel for different mesh sizings.

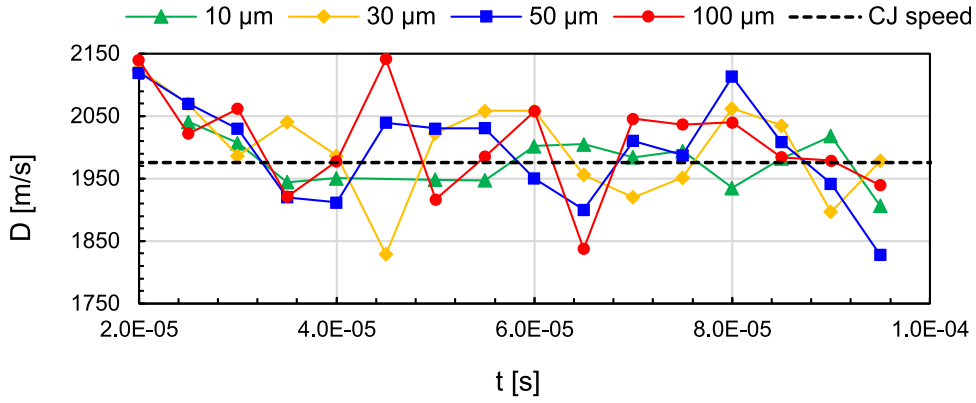

Fig. A.5. Time trends of the leading shock speed in a 2D detonation channel at a fixed transverse position for different element sizings.

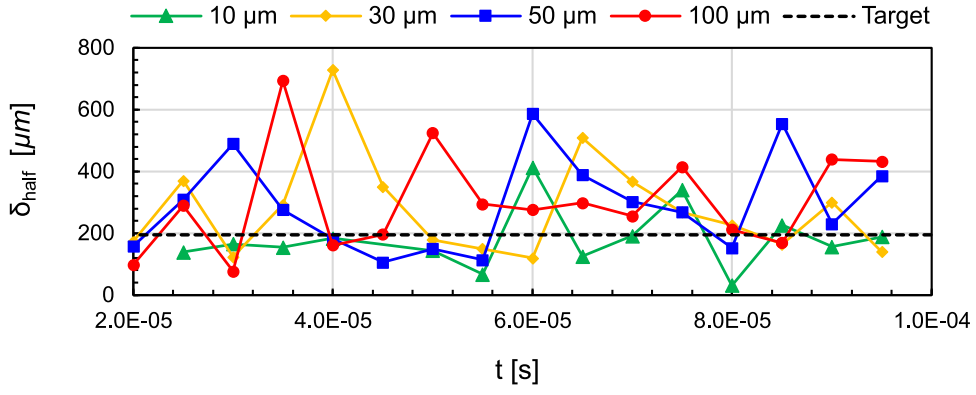

Fig. A.6. Time trends of the half reaction thickness in a 2D detonation channel at a fixed transverse position for different element sizings.

terms of spatial discretization is thus the refilled gas rather than the products in the combustion chamber. Considering that low index values are only observed where the shocks occur, the spatial discretization appears adequate for the resolution of the flow field.

To investigate the effect of the element size on the sole detonation propagation, preliminary LES simulations of a detonation propagation in a 2D channel filled with H_2-air mixture in ambient, stoichiometric conditions were carried out. The instantaneous results are reported in Fig. A.4.

As the mesh is coarsened, the smallest structures in the flow field are lost and the cellular structure becomes slightly more regular. However, the differences in the cell size and detonation front are limited when the element size is increased by one order of magnitude. The detonation speed and the half reaction thickness are also calculated at a fixed horizontal position. The values, reported in Figs. A.5 and A.6 respectively, do not change considerably with the mesh coarsening.

These observations indicate that the detonation front description is not expected to deteriorate significantly when using an element size comparable to the half reaction thickness.

References

[1] P. Stathopoulos, Comprehensive thermodynamic analysis of the Humphrey cycle for gas turbines with pressure gain combustion, Energies 11 (12) (2018) 3521, doi:10.3390/en11123521.

[2] J. Sousa, G. Paniagua, E. Collado Morata, Thermodynamic analysis of a gas turbine engine with a rotating detonation combustor, Appl. Energy 195 (2017) 247–256, doi:10.1016/j.apenergy.2017.03.045.

[3] P. Wolański, Detonative propulsion, Proc. Combust. Inst. 34 (1) (2013) 125–158, doi:10.1016/j.proci.2012.10.005.

[4] S.M. Frolov, V.S. Aksenov, V.S. Ivanov, I.O. Shamshin, Large-scale hydrogen-air continuous detonation combustor, Int. J. Hydrogen Energy 40 (3) (2015) 1616–1623, doi:10.1016/j.ijhydene.2014.11.112.

[5] A. Lentsch, R. Bec, L. Serre, F. Falempin, D. Daniau, D. Piton, A. Prigent, G. Canteins, R. Zitoun, D. Desbordes, F. Jouot, I. Gokalp, Overview of current French activities on PDRE and continuous detonation wave rocket engines (2012). 10.2514/6.2005-3232

[6] B.A. Rankin, D.R. Richardson, A.W. Caswell, A.G. Naples, J.L. Hoke, F.R. Schauer, Chemiluminescence imaging of an optically accessible non-premixed rotating detonation engine, Combust. Flame 176 (2017) 12–22, doi:10.1016/j.combustflame.2016.09.020.

[7] K. Ishihara, Y. Kato, K. Matsuoka, J. Kasahara, A. Matsuo, I. Funaki, Thrust performance evaluation of a rotating detonation engine with a conical plug, 25th ICDERS (2015), pp. 1–12.

[8] Y.-T. Shao, M. Liu, J.-P. Wang, Numerical investigation of rotating detonation engine propulsive performance, Combust. Sci. Technol. 182 (11–12) (2010) 1586–1597, doi:10.1080/00102202.2010.497316.

[9] E. Bach, P. Stathopoulos, C.O. Paschereit, M.D. Bohon, Performance analysis of a rotating detonation combustor based on stagnation pressure measurements, Combust. Flame 217 (2020) 21–36, doi:10.1016/j.combustflame.2020.03.017.

[10] V. Anand, E. Gutmark, Rotating detonation combustors and their similarities to rocket instabilities, Prog. Energy Combust. Sci. 73 (2019) 182–234, doi:10.1016/j.pecs.2019.04.001.

[11] S. Prakash, V. Raman, C.F. Lietz, W.A. Hargus, S.A. Schumaker, Numerical simulation of a methane-oxygen rotating detonation rocket engine, Proc. Combust. Inst. 38 (3) (2021) 3777–3786, doi:10.1016/j.proci.2020.06.288.

[12] D. Schwer, K. Kailasanath, Numerical investigation of the physics of rotating-detonation-engines, Proc. Combust. Inst. 33 (2) (2010) 2195–2202, doi:10.1016/j.proci.2010.07.050.

[13] N. Tsuboi, Y. Watanabe, T. Kojima, A.K. Hayashi, Numerical estimation of the thrust performance on a rotating detonation engine for a hydrogen-oxygen mixture, Proc. Combust. Inst. 35 (2) (2015) 2005–2013, doi:10.1016/j.proci.2014.09.010.

[14] M. Hishida, T. Fujiwara, P. Wolanski, Fundamentals of rotating detonations, Shock Waves 19 (1) (2009) 1–10, doi:10.1007/s00193-008-0178-2.

[15] D.A. Schwer, K. Kailasanath, Effect of inlet on fill region and performance of rotating detonation engines, 47th AIAA/ASME/SAE/ASEE Joint Propulsion Conference and Exhibit 2011 (2011), pp. 1–17, doi:10.2514/6.2011-6044.

[16] N. Tsuboi, S. Eto, A.K. Hayashi, T. Kojima, Front cellular structure and thrust performance on hydrogen-oxygen rotating detonation engine, J. Propul. Power 33 (1) (2017) 100–111, doi:10.2514/1.B36095.

[17] A.V. Dubrovskii, V.S. Ivanov, S.M. Frolov, Three-dimensional numerical simulation of the operation process in a continuous detonation combustor with separate feeding of hydrogen and air, Russian J. Phys. Chem. B 9 (1) (2015) 104–119, doi:10.1134/S1990793115010157.

[18] P.A. Cocks, A.T. Holley, B.A. Rankin, High fidelity simulations of a non-premixed rotating detonation engine, 54th AIAA Aerospace Sciences Meeting (2016), pp. 1–18, doi:10.2514/6.2016-0125.

[19] T. Gaillard, D.M. Davidenko, A.N. Kudryavtsev, I. Gökalp, Numerical simulation of a rotating detonation under conditions of premixed and separate injection of H2-O2, EUCASS (2017) 1–14, doi:10.13009/EUCASS2017-171.

[20] T. Sato, V. Raman, Detonation structure in ethylene/air based non-premixed rotating detonation engine, AIAA SciTech Forum, 2019, doi:10.2514/6.2019-2023.

[21] C.F. Lietz, Y. Desai, W. Hargus, V. Sankaran, Parametric investigation of rotating detonation rocket engines using large eddy simulations, AIAA Propulsion and Energy Forum and Exposition, 2019, 2019, doi:10.2514/6.2019-4129.

[22] T. Sato, F. Chacon, L. White, V. Raman, M. Gamba, Mixing and detonation structure in a rotating detonation engine with an axial air inlet, Proc. Combust. Inst. 38 (3) (2021) 3769–3776, doi:10.1016/j.proci.2020.06.283.

[23] A. Batista, M.C. Ross, C. Lietz, W.A. Hargus, Descending modal transition dynamics in a large eddy simulation of a rotating detonation rocket engine, Energies 14 (12) (2021) 1–22, doi:10.3390/en14123387.

[24] V. Athmanathan, J. Braun, Z.M. Ayers, C.A. Fugger, A.M. Webb, M.N. Slipchenko, G. Paniagua, S. Roy, T.R. Meyer, On the effects of reactant stratification and wall curvature in non-premixed rotating detonation combustors, Combust. Flame 240 (2022) 112013, doi:10.1016/j.combustflame.2022.112013.

[25] J.E. Shepherd, Detonation in gases, Proc. Combust. Inst. 32 I (1) (2009) 83–98, doi:10.1016/j.proci.2008.08.006.

[26] R. Bluemner, M.D. Bohon, C.O. Paschereit, E.J. Gutmark, Counter-rotating wave mode transition dynamics in an RDC, Int. J. Hydrogen Energy 44 (14) (2019) 7628–7641, doi:10.1016/j.ijhydene.2019.01.262.

[27] M.D. Bohon, A. Orchini, R. Bluemner, C.O. Paschereit, E.J. Gutmark, Dynamic mode decomposition analysis of rotating detonation waves, Shock Waves 31 (2021) 637–649, doi:10.1007/s00193-020-00975-8.

[28] R. Bluemner, M.D. Bohon, C.O. Paschereit, E.J. Gutmark, Effect of inlet and outlet boundary conditions on rotating detonation combustion, Combust. Flame 216 (2020) 300–315, doi:10.1016/j.combustflame.2020.03.011.

[29] S. Weiss, M.D. Bohon, C.O. Paschereit, E.J. Gutmark, Computational study of reactants mixing in a rotating detonation combustor using compressible RANS, Flow Turbul. Combust. 105 (2020) 267–295, doi:10.1007/s10494-019-00097-x.

[30] R. Bluemner, M.D. Bohon, C.O. Paschereit, E.J. Gutmark, Experimental study of reactant mixing in model rotating detonation combustor geometries, Flow Turbul. Combust. 102 (2) (2019) 255–277, doi:10.1007/s10494-018-9966-7.

[31] E. Bach, C.O. Paschereit, P. Stathopoulos, M.D. Bohon, An empirical model for stagnation pressure gain in rotating detonation combustors, Proc. Combust. Inst. 38 (3) (2021) 3807–3814, doi:10.1016/j.proci.2020.07.071.

[32] F. Ducros, N. Franck, T. Poinsot, Wall-adapting local eddy-viscosity models for simulations in complex geometries, Numer. Methods Fluid Dyn. VI (1998).

[33] S. Bane, J. Ziegler, J. Shepherd, Development of one-step chemistry models for flame and ignition simulation, 2010.

[34] P. Boivin, C. Jiménez, A.L. Sánchez, F.A. Williams, An explicit reduced mechanism for H2-air combustion, Proc. Combust. Inst. 33 (1) (2011) 517–523, doi:10.1016/j.proci.2010.05.002.

[35] M.C. Krejci, O. Mathieu, A.J. Vissotski, S. Ravi, T.G. Sikes, E.L. Petersen, A. Kérmonès, W. Metcalfe, H.J. Curran, Laminar flame speed and ignition delay time data for the kinetic modeling of hydrogen and syngas fuel blends, J. Eng. Gas Turbine Power 135 (2) (2013) 1–9, doi:10.1115/1.4007737.

[36] D. Davidenko, I. Gökalp, E. Dufour, P. Magre, Numerical simulation of hydrogen supersonic combustion and validation of computational approach, 12th AIAA International Space Planes and Hypersonic Systems and Technologies (2003), pp. 1–11, doi:10.2514/6.2003-7033.

[37] T. Schönfeld, M. Rudgyard, Steady and unsteady flow simulations using the hybrid flow solver AVBP, AIAA J. 37 (11) (1999) 1378–1385, doi:10.2514/2.636.

[38] P.D. Lax, B. Wendroff, Difference schemes for hyperbolic equations with high order of accuracy, Commun. Pure Appl. Math. 17 (3) (1964) 381–398, doi:10.1002/cpa.3160170311.

[39] S. Kawai, S.K. Lele, Localized artificial diffusivity scheme for discontinuity capturing on curvilinear meshes, J. Comput. Phys. 227 (22) (2008) 9498–9526, doi:10.1016/j.jcp.2008.06.034.

[40] I.B. Celik, Z.N. Cehreli, I. Yavuz, Index of resolution quality for large eddy simulations, J. Fluids Eng. Trans. ASME 127 (5) (2005) 949–958, doi:10.1115/1.1990201.

[41] J.R. Burr, K.H. Yu, Experimental characterization of RDE combustor flowfield using linear channel, Proc. Combust. Inst. 37 (3) (2019) 3471–3478, doi:10.1016/j.proci.2018.09.001.

[42] J. Fujii, Y. Kumazawa, A. Matsuo, S. Nakagami, K. Matsuoka, J. Kasahara, Numerical investigation on detonation velocity in rotating detonation engine chamber, Proc. Combust. Inst. 36 (2) (2017) 2665–2672, doi:10.1016/j.proci.2016.06.155.

[43] S. Prakash, R. Fiévet, V. Raman, J. Burr, K.H. Yu, Analysis of the detonation wave structure in a linearized rotating detonation engine, AIAA J. 58 (12) (2020) 5063–5077, doi:10.2514/1.J058156.

[44] E. Van Driest, Turbulent boundary layer in compressible fluids, J. Aeronaut. Sci. 18 (3) (1951), doi:10.2514/8.1895.

[45] R. Bluemner, Operating mode dynamics in rotating detonation combustors, Technische Universität Berlin, 2020 Ph.D. thesis. https://depositonce.tu-berlin.de/handle/11303/11517

[46] S. Browne, J. Ziegler, J.E. Shepherd, Numerical solution methods for shock and detonation jump conditions, GALCIT Tech Report FM2006.006, 2008.

[47] D.G. Goodwin, R.L. Speth, H.K. Moffat, B.W. Weber, Cantera: an object-oriented software toolkit for chemical kinetics, thermodynamics, and transport processes, 2021, https://www.cantera.org, Version 2.4.0. 10.5281/zenodo.4527812
[48] T. Sato, S. Voelkel, V. Raman, Detailed chemical kinetics based simulation of detonation-containing flows, Proceedings of the ASME Turbo Expo 2018: Volume 4A: Combustion, Fuels, and Emissions (2018), doi:10.1115/gt2018-75878.
[49] S. Prakash, V. Raman, The effects of mixture preburning on detonation wave propagation, Proc. Combust. Inst. 38 (3) (2021) 3749–3758, doi:10.1016/j.proci.2020.06.005.
[50] T.A. Kaemming, D.E. Paxson, Determining the pressure gain of pressure gain combustion, AIAA 2018-4567. 2018 Joint Propulsion Conference (2018), doi:10.2514/6.2018-4567.
[51] C.M. Brophy, J.R. Codoni, J.A. Teneyck, S. Ewing, Experimental performance characterization of an RDE using equivalent available pressure, AIAA Propulsion and Energy Forum and Exposition, 2019, 2019, doi:10.2514/6.2019-4212.
[52] E. Bach, C.O. Paschereit, P. Stathopoulos, M. Bohon, RDC operation and performance with varying air injector pressure loss, AIAA SciTech 2020 Forum, 2020, doi:10.2514/6.2020-0199.
[53] T.F. Fric, Effects of fuel-air unmixedness on NOx emissions, AIAA/ASME/SAE/ASEE 28th Joint Propulsion Conference and Exhibit, 1992, vol. 9 (1992), doi:10.2514/6.1992-3345.
[54] V. Rodriguez, C. Jourdain, P. Vidal, R. Zitoun, An experimental evidence of steadily-rotating overdriven detonation, Combust. Flame 202 (2019) 132–142, doi:10.1016/j.combustflame.2019.01.016.
[55] T. Kluge, M. Henke, J.R. Seume, Comparison of different methods for the analysis of time-resolved flow field measurements in an axial turbine, 11th European Conference on Turbomachinery Fluid Dynamics and Thermodynamics, ETC 2015 (2015), pp. 1–12.
[56] P.C. Nassini, High-fidelity numerical investigations of a hydrogen rotating detonation combustor, University of Florence, 2022 Ph.D. thesis. http://hdl.handle.net/2158/1276841
[57] J.R. Burr, K. Yu, Detonation wave propagation in cross-flow of discretely spaced reactant jets, 53rd AIAA/SAE/ASEE Joint Propulsion Conference (2017), doi:10.2514/6.2017-4908.